containing genes involved in alcohol metabolism. In addition, we found a strong genetic-environmental interaction related to the risk of OSCC. Subjects with two environmental risk factors (ever-smokers and ever-drinkers) in combination with two genetic risk factors (AA or GA at rs1229984 (*ADH1B*) and GG at rs671 (*ALDH2*)) had a much higher risk than other subjects. Specifically, compared with no risk factor, the ORs with one, two, three and four risk factors were 1.4 (95% CI 0.7 to 2.7), 4.3 (95% CI 2.2 to 8.4), 41.0 (95% CI 20.2 to 83.3), and 357.1 (95% CI 105.4 to 1209.5), respectively. Of all of the risk factors for OSCC that we had previously examined, the combination of all four factors studied had the highest risk, with an OR of 357.1.

This information on the strong genetic-environmental interaction is valuable for secondary prevention of OSCC. When we see subjects who show *ADH1B* (rs1229984) and *ALDH2* (rs671) variants as well as smoking and drinking habits, we will advise them to have a periodic upper gastrointestinal fibre test. Screening of these patients could have an important role in the early detection of OSCC. Furthermore, the information gained from this study may also enable the development of a primary individualised prevention strategy for young people with these genetic variations. When subjects have these high-risk variants, advising them not to start smoking or, especially, not to drink alcohol will dramatically reduce their risk of developing OSCC. We observed that drinkers who consumed alcohol daily and heavy smokers had higher ORs than their counterparts, and the ORs decreased with an increased amount of time since quitting these habits. However, all ORs among ever-drinkers/smokers were significantly higher than 1.0 (supplementary table 2). At present, we cannot unequivocally determine the preventive effect of quitting smoking or drinking alcohol. To determine whether stopping these habits reduces the risk of OSCC, prospective studies are needed.

Several limitations of this study should be mentioned. First, the statistical power of this genome-wide association study was not sufficient for allelic variants with an OR of <1.5 (supplementary table 1). Therefore, we might have missed variants with a small effect size (eg, 1.1–1.3), which are often reported for other lifestyle-related diseases. Second, we did not match the cases and controls; thus, the basic distributions of sex, place of residence and age were different between the two groups (table 1). However, although matching is efficient in data collection, it does not affect the point estimation if the factor is included in the model. Thus, the absence of matching did not distort the results. Third, personalised genetic testing is prohibitively expensive and ethically problematic. Finally, because of the retrospective study design, several answers in the questionnaire could be altered by disease or pre-disease conditions. Thus, the high OR among former drinkers and smokers who had quit less than 1 year previously may incorrectly imply a causal relationship between these habits and OSCC risk. Therefore, the effect of quitting these habits on OSCC risk should be examined by prospective studies.

Hashibe *et al* identified the variation of *ADH1B* (rs1229984) as a risk factor for OSCC.[10] They conducted their analysis on European and Latin American populations, and the result was consistent with the results of our study of Japanese patients and controls. A study of Chinese people also demonstrated that *ADH1B* (rs1229984) is a risk factor for OSCC.[11] Recently, Cui *et al* reported that variations of *ADH1B* (rs1229984) and *ALDH2* (rs671) coupled with alcohol drinking and smoking synergistically enhance oesophageal cancer risk.[12] Their study indicates that these two genetic risk variants provide almost equal risk for the generation of OSCC. In our study, among individuals without a genetic risk; alcohol consumption did not increase the OR of OSCC significantly. For people without genetic risk, smoking habits were the major contributing factor for the generation of OSCC. However, in people with genetic risk, a drinking habit strikingly increased the risk of OSCC; combined with smoking, it increased the risk even further (table 3).

Smoking- and alcohol drinking-related genes such as the *ADH* family, the *ALDH* family and nicotinic acetylcholine receptors, especially as indicated in SNP analyses, have been significantly associated with a variety of cancers[10 13–15] We performed an association analysis between OSCC and SNPs in the nicotinic acetylcholine receptor subunit genes *CHRNA3* and *CHRNA5* at 15q25 using the same cases and controls. An association with lung cancer was reported by Hung *et al*[14] and Thorgeirsson et *al*[13] However, in this study, we did not find a significant association at either rs1051730 (*CHRNA3*) or rs16969968 (*CHRNA5*), with ORs of 0.91 and 0.89, respectively (supplementary table 3). Smoking habits contributed to the development of OSCC; however, SNPs other than rs1051730 (*CHRNA3*) or rs16969968 (*CHRNA5*) might affect OSCC generation. Because the risk allele frequency of both of these SNPs was <0.02 in cases and controls in this study population, it would be difficult to show any difference between cases and controls. Variants of *ECRG1* have been reported to be associated with OSCC.[16] However, it is still unclear whether the genetic or epigenetic changes caused by smoking and/or alcohol drinking are directly associated with the development of OSCC in cooperation with SNPs of genes such as those of the ADH family, the ALDH family and nicotinic acetylcholine receptors[5 17] ADH1B in subjects with the rs1229984 AA or GA genotype is reported to metabolise ethanol up to 40 times more quickly than ADH1B from GG homozygotes.[18] Furthermore, ALDH2 from subjects with the GG allele of rs671 is reported to metabolise acetaldehyde more than 100 times faster than from AG ALDH2 heterozygotes.[19] In addition, *ADH* genes exhibit a nominally significant association with smoking behaviour.[20] Considering our results and these reports, higher local exposure to ethanol and acetaldehyde mediated by smoking may be strongly associated with OSCC development. To answer these questions, it is necessary to conduct a prospective study in genetically at-risk populations with or without drinking and/or smoking habits, as recently performed for type 2 diabetes.[21 22]

In summary, this study disclosed a significant genetic-environmental interaction, with very large ORs, associated with the development of OSCC. Thus, convincing young people to smoke and drink less is likely to reduce the incidence of OSCC. SNP genotyping demonstrated that the *ADH1B* and/or *ALDH2* risk alleles had an interaction with smoking and, especially, alcohol consumption. Analysis of *ADH1B* and *ALDH2* variants would be valuable for secondary prevention of OSCC in high-risk patients who smoke and drink alcohol. Our findings, if replicated in other groups, could demonstrate new pathophysiological pathways for the development of OSCC.

Acknowledgements We thank Ms. Judith Clayton for her critical reading of the manuscript.

Funding This work was supported in part by the following grants and foundations: Japan Society for the Promotion of Science (JSPS) Grant-in-Aid for Scientific Research, grant numbers 17109013, 21229015; CREST, Japan Science and Technology Agency (JST); NEDO (New Energy and Industrial Technology Development Organization) Technological Development for Chromosome Analysis; and The Ministry of Education, Culture, Sports, Science, and Technology of Japan for Scientific Research on Priority Areas, Cancer Translational Research Project, Japan. Other Funders: Japan Society for the Promotion of Science (JSPS) Grant-in-Aid for Scientific Research, Japan Science and Technology Agency, New Energy and Industrial Technology Development Organization.

Competing interests None.

Ethics approval This study was conducted with the approval of the Kyusyu University, Juntendo University, National Cancer Institute, Saitama Cancer Center, Kurume University, and Kurume University, Japan.

Contributors KY, SS, and H Inoue equally contributed to this study. FT, KY, MT, HK, HF, YT, SN, ST, KM, KI, ST, NH, H Ishii, H Inoue and MM jointly designed the study and organised the recruitment of participants. Y Kajiyama, H Igaki, KF, TT, Y Kawashima, and TS organised the recruitment of participants and biological samples. KY conducted the SNP study and the statistical analysis and drafted the manuscript. SS organised the environmental study and the statistical analysis and drafted the manuscript. FT had full access to all of the data in the study and takes responsibility for the integrity of the data and the accuracy of the data analysis.

Provenance and peer review Not commissioned; externally peer reviewed.

REFERENCES

1. **Shimada H,** Kitabayashi H, Nabeya Y, *et al*. Treatment response and prognosis of patients after recurrence of esophageal cancer. *Surgery* 2003;**133**:24–31.
2. **Parkin DM,** Bray F, Ferlay J, *et al*. Global cancer statistics, 2002. *CA Cancer J Clin* 2005;**55**:74–108.
3. **Brooks PJ,** Enoch MA, Goldman D, *et al*. The alcohol flushing response: an unrecognized risk factor for esophageal cancer from alcohol consumption. *PLoS Med* 2009;**6**:e50.
4. **Tsuchihashi-Makaya M,** Serizawa M, Yanai K, *et al*. Gene-environmental interaction regarding alcohol-metabolizing enzymes in the Japanese general population. *Hypertens Res* 2009;**32**:207–13.
5. **Druesne-Pecollo N,** Tehard B, Mallet Y, *et al*. Alcohol and genetic polymorphisms: effect on risk of alcohol-related cancer. *Lancet Oncol* 2009;**10**:173–80.
6. **Purcell S,** Neale B, Todd-Brown K, *et al*. PLINK: a tool set for whole-genome association and population-based linkage analyses. *Am J Hum Genet* 2007;**81**:559–75.
7. **Barrett JC,** Fry B, Maller J, *et al*. Haploview: analysis and visualization of LD and haplotype maps. *Bioinformatics* 2005;**21**:263–5.
8. **Dupont WD,** Plummer WD Jr. Power and sample size calculations. A review and computer program. *Control Clin Trials* 1990;**11**:116–28.
9. **Ishiguro S,** Sasazuki S, Inoue M, *et al*. Effect of alcohol consumption, cigarette smoking and flushing response on esophageal cancer risk: a population-based cohort study (JPHC study). *Cancer Lett* 2009;**275**:240–6.
10. **Hashibe M,** McKay JD, Curado MP, *et al*. Multiple ADH genes are associated with upper aerodigestive cancers. *Nat Genet* 2008;**40**:707–9.
11. **Yang SJ,** Wang HY, Li XQ, *et al*. Genetic polymorphisms of ADH2 and ALDH2 association with esophageal cancer risk in southwest China. *World J Gastroenterol* 2007;**13**:5760–4.
12. **Cui R,** Kamatani Y, Takahashi A, *et al*. Functional variants in ADH1B and ALDH2 coupled with alcohol and smoking synergistically enhance esophageal cancer risk. *Gastroenterology* 2009;**137**:1768–75.
13. **Thorgeirsson TE,** Geller F, Sulem P, *et al*. A variant associated with nicotine dependence, lung cancer and peripheral arterial disease. *Nature* 2008;**452**:638–42.
14. **Hung RJ,** McKay JD, Gaborieau V, *et al*. A susceptibility locus for lung cancer maps to nicotinic acetylcholine receptor subunit genes on 15q25. *Nature* 2008;**452**:633–7.
15. **Berrettini W,** Yuan X, Tozzi F, *et al*. Alpha-5/alpha-3 nicotinic receptor subunit alleles increase risk for heavy smoking. *Mol Psychiatry* 2008;**13**:368–73.
16. **Li Y,** Zhang X, Huang G, *et al*. Identification of a novel polymorphism Arg290Gln of esophageal cancer related gene 1 (ECRG1) and its related risk to esophageal squamous cell carcinoma. *Carcinogenesis* 2006;**27**:798–802.
17. **Chanock SJ,** Hunter DJ. Genomics: when the smoke clears. *Nature* 2008;**452**:537–8.
18. **Hashibe M,** Boffetta P, Zaridze D, *et al*. Evidence for an important role of alcohol- and aldehyde-metabolizing genes in cancers of the upper aerodigestive tract. *Cancer Epidemiol Biomarkers Prev* 2006;**15**:696–703.
19. **Peng GS,** Yin SJ. Effect of the allelic variants of aldehyde dehydrogenase ALDH2*2 and alcohol dehydrogenase ADH1B*2 on blood acetaldehyde concentrations. *Hum Genomics* 2009;**3**:121–7.
20. **Caporaso N,** Gu F, Chatterjee N, *et al*. Genome-wide and candidate gene association study of cigarette smoking behaviors. *PLoS ONE* 2009;**4**:e4653.
21. **Meigs JB,** Shrader P, Sullivan LM, *et al*. Genotype score in addition to common risk factors for prediction of type 2 diabetes. *N Engl J Med* 2008;**359**:2208–19.
22. **Lyssenko V,** Jonsson A, Almgren P, *et al*. Clinical risk factors, DNA variants, and the development of type 2 diabetes. *N Engl J Med* 2008;**359**:2220–32.

Editor's quiz: GI snapshot

Pizza, beer, amylase, lipase and the acute abdomen

CLINICAL PRESENTATION

A previously healthy 16-year-old male student was admitted with acute abdominal pain after eating two large pizzas and drinking five pints (approximately 2.8 l) of beer (alcohol content 4.5%). Initial assessment revealed epigastric tenderness with elevated serum amylase (380 IU/l, normal 30–110 IU/l), and lipase (4398 IU/l, normal 23–300 IU/l) concentrations. There was no free gas on the chest radiograph. The patient developed increasing abdominal pain, tenderness, tachycardia and a lactic acidosis (pH 7.20, lactate 2.91 mmol/l) within 6 h. Contrast-enhanced abdominal CT (figure 1) was done 8 h after admission.

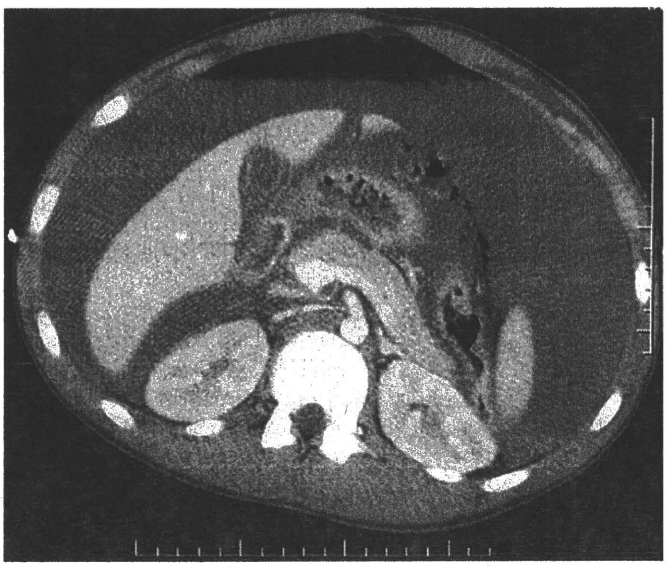

Figure 1 Contrast-enhanced CT scan of the abdomen.

QUESTION

What are the findings on CT?

See page 1560 for answer

James A Catton, Dileep N Lobo

Division of Gastrointestinal Surgery, Nottingham Digestive Diseases Centre NIHR Biomedical Research Unit, Nottingham University Hospitals, Queen's Medical Centre, Nottingham, UK

Correspondence to Mr D.N. Lobo, Division of Gastrointestinal Surgery, E Floor, West Block, Nottingham University Hospitals, Queen's Medical Centre, Nottingham NG7 2UH, UK; dileep.lobo@nottingham.ac.uk

Competing interests None.

Patient consent Obtained from parent.

Provenance and peer review Not commissioned; not externally peer reviewed.

Gut 2010;**59**:1464. doi:10.1136/gut.2009.184010

Imaging study of pancreatic ductal adenocarcinomas in Syrian hamsters using X-ray micro-computed tomography (CT)

Tsukasa Kitahashi,[1] Michihiro Mutoh,[2] Masakatsu Tsurusaki,[3] Gen Iinuma,[3] Masahiro Suzuki,[4] Noriyuki Moriyama,[4] Mitsuyoshi Yoshimoto,[2] Keiji Wakabayashi,[2] Takashi Sugimura[2] and Toshio Imai[1,5]

[1]Central Animal Laboratory, [2]Cancer Prevention Basic Research Project, National Cancer Center Research Institute, Tokyo; [3]Diagnostic Radiology Division, National Cancer Center Hospital, Tokyo; [4]Research Center for Cancer Prevention and Screening, National Cancer Center, Tokyo, Japan

(Received January 13, 2010/Revised March 19, 2010/Accepted March 29, 2010/Accepted manuscript online April 7, 2010/Article first published online April 30, 2010)

X-ray computed tomography (CT) has been used for diagnoses of human pancreatic cancer. Although micro-CT is a useful approach to evaluate macromorphology of organs/tissue also in animal models, reports on pancreatic tumors are limited. In this study, the utility of micro-CT was assessed in characterizing chemically induced pancreatic tumors in Syrian hamsters. Hamsters treated with or without *N*-nitrosobis(2-oxopropyl)amine (BOP) were injected with the antispasmodic agent, scopolamine butylbromide, and contrast agents, 5 or 10 mL/kg body weight of iopamidol or Fenestra VC at 18–38 weeks, then examined by micro-CT scanning with a respiratory gating system. Both peristaltic and respiratory movements were substantially suppressed by the combination of scopolamine butylbromide treatment and the respiratory gating system, resulting in improvements of image qualities. Iopamidol clearly visualized the pancreatic parenchyma and contrasted the margins among the pancreas and other abdominal organs/tissue. Meanwhile Fenestra VC predominantly contrasted abdominal vascular systems, but the margins among pancreas and other organs/tissue remained obscure. Six pancreatic tumors of 4–13 mm in diameter were detected in four of 15 animals, but not the five tumors of 1–4 mm in diameter. The inner tumor images were heterogeneously or uniformly visualized by iopamidol and Fenestra VC. Overall, iopamidol could clearly contrast between pancreatic parenchyma and the tumors as compared with Fenestra VC. All tumors confirmed were histopathologically diagnosed as pancreatic ductal adenocarcinomas. Thus, micro-CT could be useful to evaluate the carcinogenic processes and preventive methods of pancreatic cancer in hamsters and to assess the novel contrast agents for detection of small pancreatic cancer in humans. (*Cancer Sci* 2010; 101: 1761–1766)

Pancreatic cancer is the fifth cause of cancer death in Japan and ranks high in mortality among developed countries.[1,2] Because of the difficulty in detecting pancreatic cancer in early operable stages, and because of the lack of any curative treatment approaches other than complete surgical removal, 5-year relative survival rate is <6%.[3,4] Therefore, for improvement of outcome, future strategies for early diagnosis of pancreatic cancer should aim at diagnosing most pancreatic cancers before they grow 20 mm in size.[5,6]

X-ray computed tomography (CT) has been widely used in detection and evaluation of pancreatic tumor progression and metastasis during clinical treatment. Recently, the CT devices have been markedly improved in their volume coverage speed, longitudinal resolution, and quality of three-dimensional reformations. In addition, dynamic CT scanning has been developed, in which CT-images of pancreas can be obtained for a short time with breath holding. This method reveals some adequate contrasts between pancreatic parenchyma and neoplastic lesions.[7] However, detectability of small pancreatic cancer, especially those <10 mm in size, has not yet been satisfactory.[8–10] Further amelioration of contrasting technologies that differentiate between tumors and pancreatic parenchyma is desirable to detect small pancreatic cancer.

Micro-CT is a useful tool for monitoring tumor development in living animal models, for example utility has been reported for detection of metastatic foci of xenograft rodent models[11,12] and periodic measurement of sizes in lung tumors and their growth overtime in a chemically induced carcinogenesis model.[13] In addition, respiratory gating systems appreciably resolve the thoracic movements in lung imaging.[11,13] However, the utility of micro-CT has been limited to several organs/tissue harboring distant X-ray adsorption ranges from surrounding tissue. The X-ray adsorption range is too close among abdominal organs/tissue to observe fine structures, and not only respiratory but also intestinal peristaltic movement interferes with CT imaging. Because of these limitations, pancreatic morphology and tumor imaging have not yet been reported in experimental animals.

In the present study, hamster pancreas and chemically induced pancreatic tumors were macromorphologically investigated by micro-CT with two characteristic contrast agents, iopamidol, which is a nonionic water-soluble iodine contrast agent typically used for clinical evaluations, and Fenestra VC, which is a polyiodinated lipid emulsion with blood pool properties developed for small animals.[14] The results obtained in the present study should provide basic information for CT-imaging of the pancreas and pancreatic tumor macromorphology and location in hamsters.

Materials and Methods

Animals. A total of 19 female Syrian golden hamsters at 5 weeks of age were purchased from Japan SLC (Shizuoka, Japan). They were housed two or three to a plastic cage with woodchip bedding in an air-conditioned animal room maintained at 24 ± 2°C and 60 ± 5% relative humidity with a 12:12-h light–dark cycle. Basal diet (CE-2; CLEA Japan, Tokyo, Japan) and water were available ad libitum throughout the experiment.

Anatomical features of hamster pancreas. For anatomical references of the pancreatic location and morphology, hamsters were dissected and pancreata were excised from abdominal cavity. A representative macroscopic feature of hamster pancreas is shown in Figure 1. In hamsters, the pancreas is a soft and flat organ and consists of four compartmentalized sections of the head portion and gastric, splenic, and duodenal lobes. There were no clear borderlines among the four sections, and three

[5]To whom correspondence should be addressed. E-mail: toimai@ncc.go.jp

doi: 10.1111/j.1349-7006.2010.01588.x

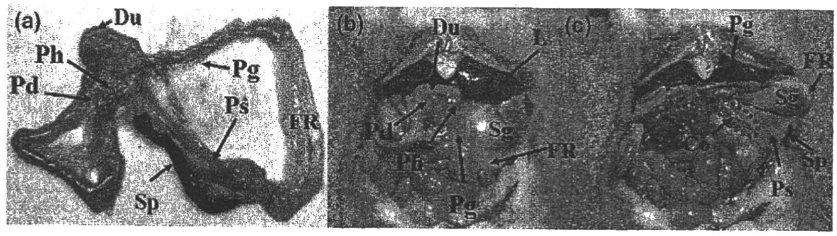

Fig. 1. Anatomical features of hamster pancreas and abdomen. (a) Pancreas excised from a hamster abdomen. (b) A hamster intra-abdomen at laparotomy and (c) behind the stomach. Red dotted circles indicate a part of gastric or splenic lobes adhered to colon. Co, colon; Du, duodenum; FR, fat ring; L, liver; Pd, pancreas duodenal lobe; Pg, pancreas gastric lobe; Ph, pancreas head; Ps, pancreas splenic lobe; Sg, glandular stomach; Sp, spleen.

lobes including gastric, splenic, and duodenal are extended from the head (Fig. 1a). The duodenal lobe is smaller than the other two lobes, and the length of this lobe is about 10 mm in an animal with 180–200 g bodyweight (BW). Gastric and splenic lobes are 20–25 mm long. The tails of both gastric and splenic lobes are bridged by adipose tissue, which is called "fat ring." Figure 1(b) shows the location of the pancreas in hamsters at laparotomy. The gastric and splenic lobes of pancreas are beside the gastric wall at the ventral and dorsal sides, respectively, (Fig. 1b,c) partially adhering to the colon (Fig. 1c, red dotted circles). The spleen is adjacent to the splenic lobe (Fig. 1a,c). The head and duodenal lobe were observed under the duodenum (Fig. 1b).

Pancreatic tumor induction. After an acclimation period of 1 week, 15 hamsters were subcutaneously injected with *N*-nitrosobis(2-oxopropyl)amine (BOP; Nacalai Tesque, Kyoto, Japan) in saline at 10 mg/kg BW four times every other day. The other four hamsters without BOP were underwent the following treatments for micro-CT imaging of normal pancreatic morphology. The experiments were conducted according to the Guidelines for Animal Experiments from the Committee for Ethics of Animal Experimentation at the National Cancer Center.

Micro-CT scan procedure. After fasting for 24 h, all hamsters with or without BOP treatment at ages from 18 to 38 weeks were anesthetized with Isoflurane (ISOFLU; Dainippon Sumitomo Pharmaceutical, Osaka, Japan) and the anesthesia was maintained with a mixture of Isoflurane and room air delivered during the micro-CT scanning.

Each hamster was placed on its back on an animal bed for micro-CT scanning. 5 mL/kg BW of iopamidol (Iopamiron 370; *N,N'*-bis[2-hydroxy-1-(hydroxymethyl)ethyl]-5-[(2S)-2-hydroxypropanoylamino]-2,4,6-triiodoisophthalamide; Bayer Shering Pharma, Osaka, Japan) (Fig. 2a), which is a nonionic iodine contrast agent for urinary tract and vascular imaging, or 10 mL/kg BW of Fenestra VC (1,3-bis-[7-(3-amino-2,4,6-triiodophenyl)heptanoyl]-2-oleoyl-glycerol; ART Advanced Research Technologies, Saint-Laurent, QC, Canada) (Fig. 2b), which is an iodinated lipids contrast agent with blood pool properties for animal imaging, were injected into cervical vein. The dose of each contrast agent was determined on the basis of the manufacturer's recommendation with modifications to obtain optimal contrasts among organs/tissue for hamster abdominal imaging. The dose of iopamidol is about three times higher than that in human cases. An intraperitoneal injection of 5 mg/kg BW of scopolamine butylbromide (Buscopan; (1S,2S,4R,5R,7s)-9-butyl-7-[(2S)-3-hydroxy-2-phenylpropanoyloxy]-9-methyl-3-oxa-9-azoniatricyclo[3.3.1.$0^{2,4}$]nonane bromide; Boehringer Ingelheim, Ingelheim, Germany), which is an antispasmodic agent diluted with saline, was then given to suppress intestinal peristaltic movement, and a sensor for detecting respiration was placed on the chin to avoid the shift of organ positions. In order to observe the precise morphology of each hamster pancreas, following the first micro-CT scanning for each animal, hamsters were injected with either of the contrast agents again after a washout period of the contrast agents for 24 h, and immediately sacrificed by cervical dislocation, and again, examined by micro-CT at 30 min after sacrifice.

The X-ray scanning time point was set at 1200 millisecond (ms) after expiration. For scanning, a cone-beam micro-CT scanner (eXplore Locus; GE Healthcare, London, UK) was used. The scan parameters that are consistent for gated *in vivo* scan acquisitions include 80 kV peak, 450 μA, 400 ms per frame, 0.5 degrees at the angle of increment, and 720 views. The measured in-air radiation at the isocenter was 240 mGy. Scanning times with and without the respiratory gating system were about 40 and 15 min, respectively. Three-dimensional images obtained from axial, sagittal, and coronal micro-CT images were reconstructed at 45 μm voxel using MicroView (GE Healthcare).

Histopathological examination. After X-ray scanning, the hamsters were autopsied. Pancreas was removed and fixed in 10% buffered formalin, and then they were embedded in paraffin, sectioned, and stained with hematoxylin–eosin (H&E) for histopathological evaluation. Pancreatic lesions were diagnosed according to the criteria described earlier.[15]

Results

Micro-CT imaging of hamster pancreas with iopamidol. A hamster abdomen was scanned by micro-CT without contrast agents. As a result, only a few major organs such as the liver, stomach, and kidneys were observed. However, pancreas and other abdominal organs/tissue were not detected by micro-CT images (data not shown). Therefore, the contrast agent, iopamidol, was administered to a hamster in order to visualize pancre-

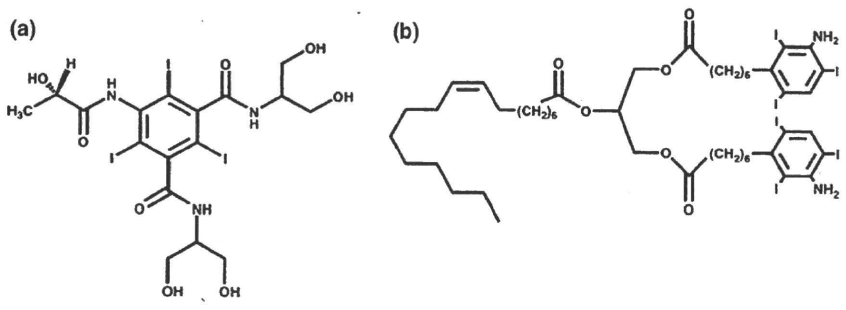

Fig. 2. Chemical structures of iopamidol (*N,N'*-bis[2-hydroxy-1-(hydroxymethyl)ethyl]-5-[(2S)-2-hydroxypropanoylamino]-2,4,6-triiodoisophthalamide) (a) and Fenestra VC (1,3-bis-[7-(3-amino-2,4,6-triiodophenyl)heptanoyl]-2-oleoyl-glycerol) (b).

doi: 10.1111/j.1349-7006.2010.01588.x

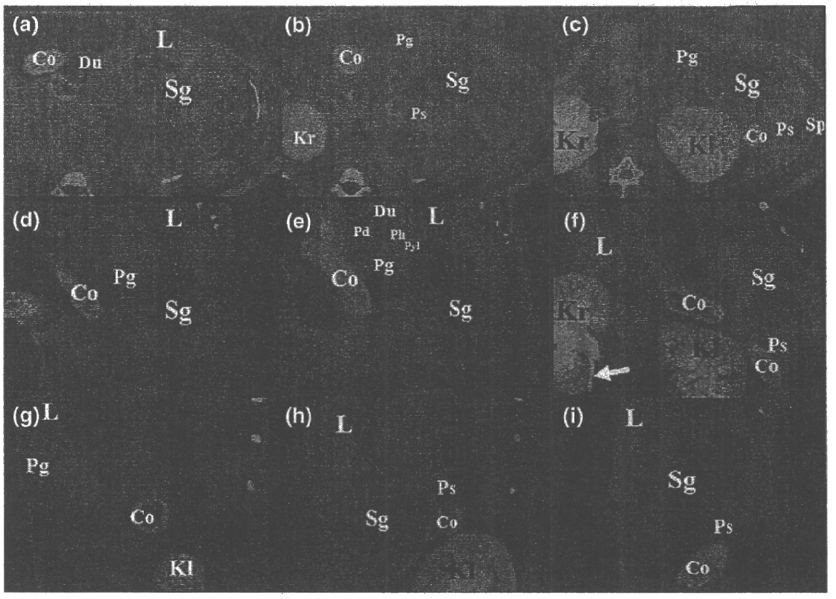

Fig. 3. The micro-computed tomography (CT) images of hamster abdomen with iopamidol. A hamster administrated with scopolamine butylbromide and iopamidol was examined by micro-CT with respiratory gating system. Each image represents axial (a–c), colonal (d–f), and sagittal (g–i) views around the pancreas. An arrow indicates iopamidol excretion into the urinary tract (f). Co, colon; Du, duodenum; Kl, left kidney; Kr, right kidney; L, liver; Pd, pancreas duodenal lobe; Pg, pancreas gastric lobe; Ph, pancreas head; Ps, pancreas splenic lobe; Pyl, Pylorus of stomach; Sg, glandular stomach; Sp, spleen.

atic images before micro-CT scanning. The liver, stomach, kidneys, spleen, colon, and duodenum were clearly visualized (Fig. 3). Some undigested food and/or wood chip residues were left in the stomach, despite fasting for 24 h. Gastric and splenic lobes of pancreas were also observed (Fig. 3b–i) by iopamidol treatment. Both gastric and splenic lobes of pancreas were located on the ventral and dorsal side, respectively, of gastric wall (Fig. 3b,c) and spleen was adjacent to the splenic lobe (Fig. 3c). The head and duodenal lobe of pancreas were located under the duodenum (Fig. 3e) and colon was adjacent to the duodenal, gastric, and splenic lobes (Fig. 3e,f,h,i). Each sagittal view in Figure 3 also visualized gastric and splenic lobes on the ventral and dorsal sides of stomach (Fig. 3g–i). To summarize the configuration of pancreatic sections on micro-CT images, the head beside the pylorus was medial, and the gastric and splenic lobes lay directly anterior and posterior to the antrum of stomach, respectively, and the duodenal lobe of the pancreas was inferior to the duodenum. In Figure 3(c,f), artifacts appear as radial white lines in the renal medulla and cortex, and renal papilla and ureter were intensely contrasted by iopamidol concentration.

Micro-CT scanning required at least several minutes. In addition to both respiratory and peristaltic movements, excretion of contrast agents during micro-CT scanning is thought to cause the contrast degradations in each organs/tissue. In order to detect the precise location and structure of pancreas by micro-CT, hamsters were treated with iopamidol again and immediately sacrificed to stop both respiratory and peristaltic movement and excretion of iopamidol, and then hamsters were examined by micro-CT scanning. Distinct contrasts in parenchyma among organs/tissue and the sharp edge of the liver, stomach, kidneys, esophagus, duodenum, and all pancreatic sections were clearly visualized in a sacrificed animal (Fig. 4) and compared with the images of a living animal shown in Figure 3. As well as the anatomical information in Figure 1, the head and duodenal lobe of the pancreas were located under the pylorus and duodenum, respectively, (Fig. 4e) and the gastric and splenic lobes were located beside the gastric wall (Fig. 4b–d,f–i) and they were also adjacent to the colon (Fig. 4e,f). In addition to main abdominal vascular systems of the inferior vena cava (IVC) and aorta (Ao), part of the blood vessels in the pancreatic parenchyma was also visualized (Fig. 4d, arrowheads). Radial artifacts in the renal

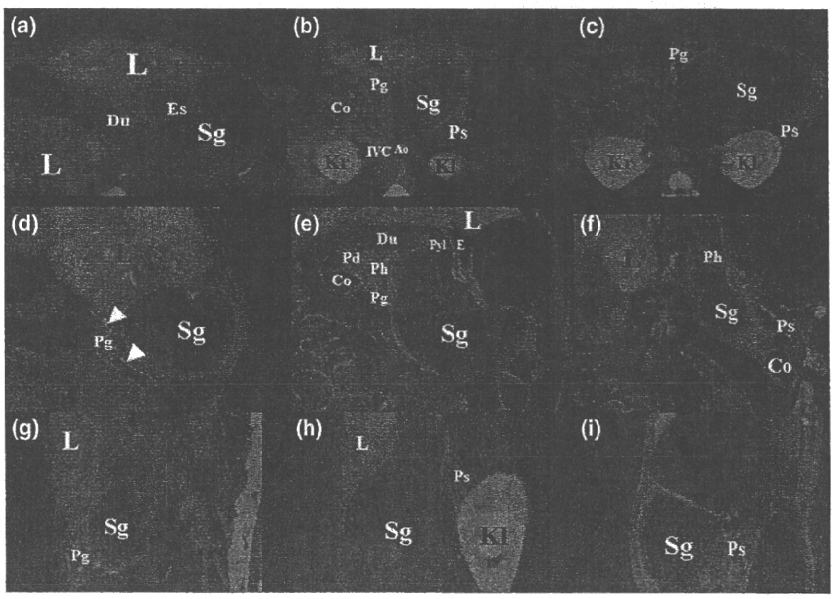

Fig. 4. The micro-computed tomography (CT) images of hamster abdomen with iopamidol after sacrifice. A hamster administrated with iopamidol was immediately sacrificed and was examined by micro-CT. Each image represents axial (a–c), colonal (d–f), and sagittal (g–i) views around pancreas. Arrowheads indicate the blood vessel in the pancreatic parenchyma (d). Co, colon; Du, duodenum; Es, esophagus; Kl, left kidney; Kr, right kidney; L, liver; Pg, pancreas gastric lobe; Ph, pancreas head; Ps, pancreas splenic lobe; Pyl, pylorus of stomach; Sg, glandular stomach.

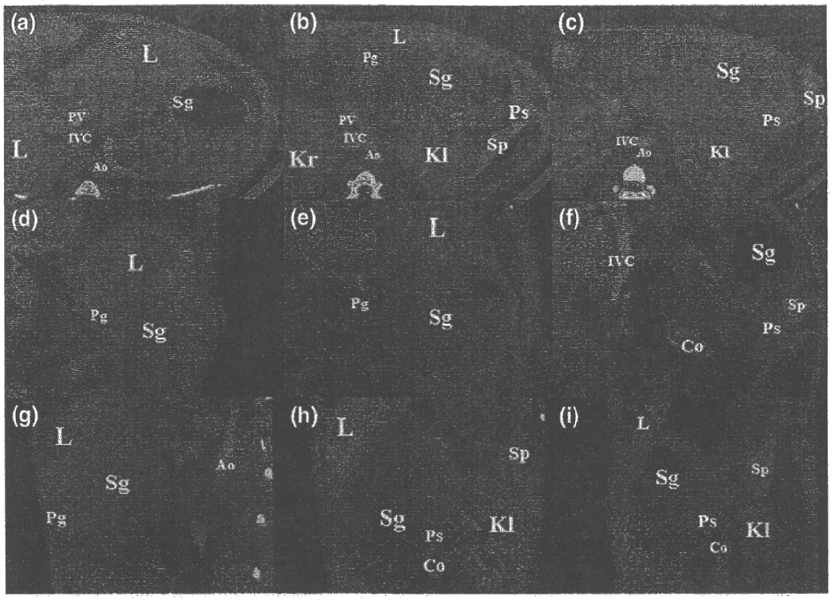

Fig. 5. The micro-computed tomography (CT) images of hamster abdomen with Fenestra VC. A hamster administrated with Buscopan and Fenestra VC was examined by micro-CT with the respiratory gating system. Images depict axial (a–c), colonal (d–f), and sagittal (g–i) views around pancreas. Ao, aorta; Co, colon; IVC, inferior vena cava; Kl, left kidney; Kr, right kidney; L, liver; Pg, pancreas gastric lobe; Ps, pancreas splenic lobe; PV, portal vein; Sg, glandular stomach; Sp, spleen.

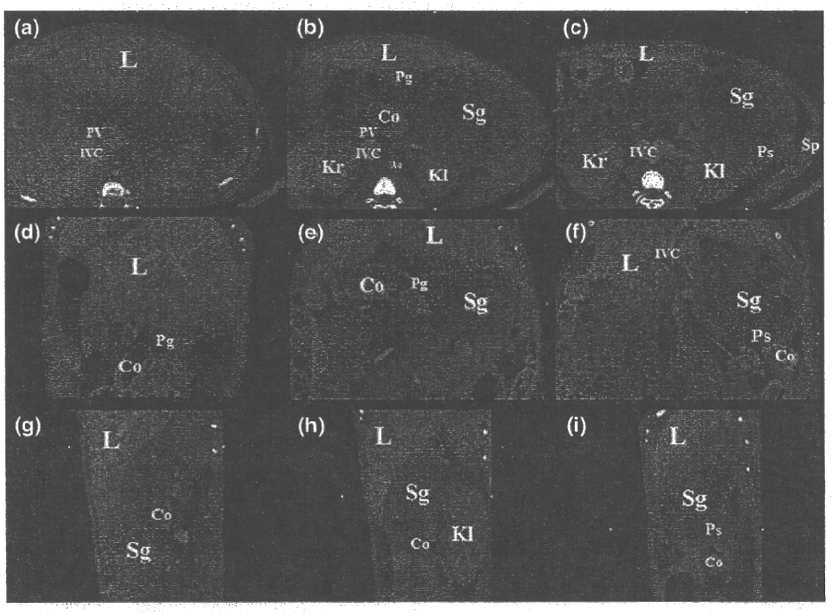

Fig. 6. The micro-computed tomography (CT) images of hamster abdomen with Fenestra VC after sacrifice. A hamster administrated with Fenestra VC was immediately sacrificed and was examined by micro-CT. Images depict axial (a–c), colonal (d–f), and sagittal (g–i) views around pancreas. Ao, aorta; Co, colon; IVC, inferior vena cava; Kl, left kidney; Kr, right kidney; L, liver; Pg, pancreas gastric lobe; Ps, pancreas splenic lobe; PV, portal vein; Sg, glandular stomach; Sp, spleen.

medulla and cortex and iopamidol concentration into renal papilla and ureter were not observed.

Micro-CT imaging of hamster pancreas with Fenestra VC. Figure 5 shows the Fenestra VC-visualized micro-CT images in hamster abdomen. Administration of Fenestra VC clearly contrasted abdominal vascular systems, such as portal vein (PV), IVC, and Ao (Fig. 5a–c,f,g). The gastric and splenic lobes of the pancreas were visualized on the same positions as those visualized by iopamidol in Figure 3. However, the border and the parenchyma of the organs/tissue were not clearly differentiated in comparison to the images made visible with iopamidol. Figure 6 shows a sacrificed hamster abdominal image contrasted with Fenestra VC. The edges of each abdominal organ, such as the liver, stomach, kidneys, and blood vessels, were improved to some extent as compared with the images in a living animal (Fig. 6). The contrasts among organs/tissue parenchyma did not seem to change. Fenestra VC was likely retained in blood vessels during micro-CT imaging for 40 min.

Micro-CT imaging of hamster pancreatic tumors. A total of 15 BOP-treated hamsters were examined by micro-CT. Groups of eight and seven hamsters were administered with iopamidol and Fenestra VC, respectively. A total of six pancreatic tumors of 4–13 mm in diameter were visualized with iopamidol or Fenestra VC in four of 15 animals from 18 to 38 weeks old. Micro-CT scanning with iopamidol visualized four tumors of 4, 6, 7, and 10 mm in diameter in two animals. The tumors of 4 and 6 mm in diameter numbered 1 and 2 (#1 and #2) developed in one animal shown in Figure 7(a,b). A poorly defined heterogeneously visualized mass-like image of 4 mm in diameter, which was confirmed to be a tumor #1 in an autopsy finding (dotted black circle of Fig. 7a), was observed in the body of the gastric lobe (Fig. 7e). Tumor #2 showed a hypoattenuating mass image of 6 mm in diameter with a clear margin compared with surrounding pancreatic parenchyma in the pancreatic body of the splenic lobe (Fig. 7b,e). The other tumors of 7 and 10 mm in diameter developed in another animal and also were visible as heterogeneous masses in the gastric and splenic lobes, respectively (data not shown). All these four tumors were diagnosed as pancreatic ductal adenocarcinomas. Tumors #1 and #2 were moderately differentiated tubular adenocarci-

doi: 10.1111/j.1349-7006.2010.01588.x

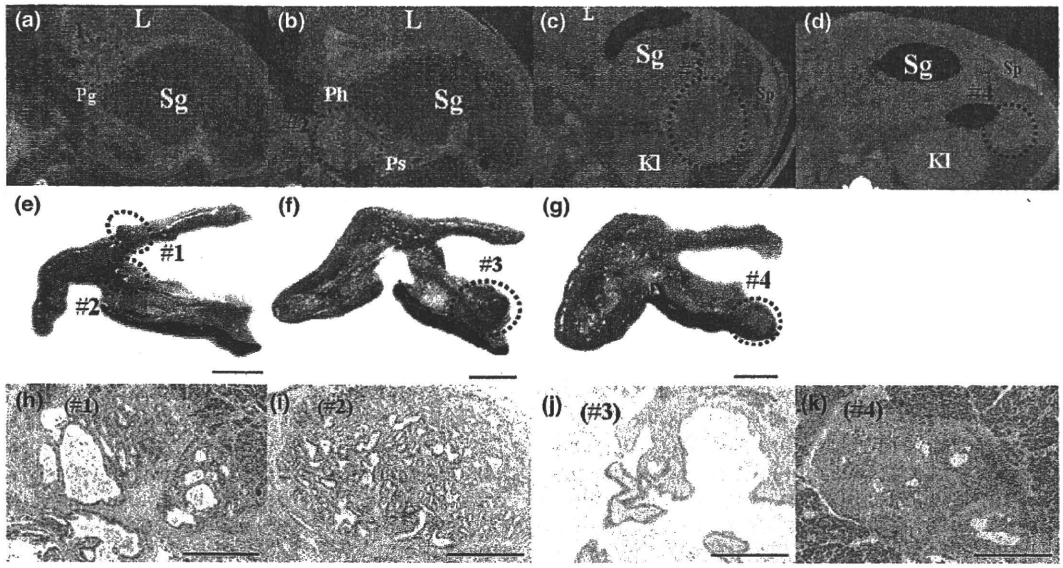

Fig. 7. Representative images of hamster pancreatic tumors. Micro-computed tomography (CT) images visualized with iopamidol and Fenestra VC are shown in (a–d) respectively. Tumors in dotted circles in (a–d) are numbered 1–4 (tumors #1–4), respectively. Macroscopic and microscopic features stained with H&E from tumors #1–4 are shown in (e–g) and (h–k), respectively. (e–g) Scale bar = 10 mm. (h–k) Scale bar = 500 μm. Kl, left kidney; L, liver; Pg, pancreas gastric lobe; Ph, pancreas head; Ps, pancreas splenic lobe; Sg, glandular stomach; Sp, spleen.

nomas (Fig. 7h,i). The other two tumors were moderately differentiated tubular adenocarcinoma and poorly differentiated adenocarcinoma with abundant stromal formation (data not shown). In addition to the above-mentioned four tumors detected by micro-CT with iopamidol, two moderately differentiated small adenocarcinomas of 1 and 0.5 mm in diameter each were histopathologically confirmed in the head of the pancreas of another animal, while these ones were not detected by micro-CT imaging with iopamidol.

Micro-CT scanning with Fenestra VC revealed two tumors of 13 and 10 mm in diameter (tumors #3 and #4) in two animals each (Fig. 7c,d). Both tumors #3 and #4 were observed in the tails of splenic lobes. Both tumor contrasts were slightly attenuated as compared with pancreatic parenchyma and the images of inner tumors were uniformly made visible with Fenestra VC. At autopsy, two tumors were found in similar positions (Fig. 7f,g) and histopathologically diagnosed as pancreatic ductal adenocarcinomas (Fig. 7j,k). Tumor #3 was cystadenocarcinoma (Fig. 7j) and tumor #4 was poorly differentiated adenocarcinoma with abundant stromal formation (Fig. 7k). In addition to these two tumors, three adenocarcinomas of 4, 1, and 1 mm in diameter were histopathologically confirmed in the gastric lobes of pancreas in other hamsters, while these ones were not detected by micro-CT imaging with Fenestra VC. These three adenocarcinomas were poorly differentiated adenocarcinomas with stromal formation (data not shown).

In addition to pancreatic ductal carcinogenic changes, moderate fatty infiltrations were also histopathologically observed in pancreatic parenchyma of all the BOP-treated hamsters. However, no significant contrast changes in pancreatic parenchyma were found by micro-CT imaging among hamsters with and without BOP (Figs 3,5,7a–d).

Discussion

In the present study, pancreatic morphology and chemically induced pancreatic tumors in Syrian hamsters were shown to be detectable by micro-CT. The Syrian hamster model with BOP has been widely applied as an animal model for the study of human pancreatic ductal carcinogenesis and data showing morphological details of both the early and advanced lesions have been reported.[15–17]

In order to substantially suppress the respiratory and the peristaltic movements during CT scanning, the antispasmodic agent, scopolamine butylbromide, was administered in combination with the respiratory gating system. The respiratory gating system improved and reduced motion artifacts caused by respiratory movements on the present scanning parameter. The images of abdomen without scopolamine butylbromide treatment were not clearly visible, especially at the edge of organs/tissue, as compared with the images using scopolamine butylbromide (data not shown). The 5 mg/kg BW dose of scopolamine butylbromide is about 15 times higher than that in human cases. No toxicological data of scopolamine butylbromide in hamsters is available, but lethal dose 50% (LD_{50}) of scopolamine butylbromide in an intravenous administration study in mice was estimated to 20 mg/kg BW (manufacturer's in-house data), which is four times higher than the present dose. Therefore, it is likely that a single or short-term repeated intraperitoneal administration of scopolamine butylbromide at the present dose might be safe for administration. Although causes of the difference in adequate doses between hamsters and humans are unclear, application of both scopolamine butylbromide and the respiratory gating system is considered to be a useful method for abdominal imaging in animal models.

In the present study, two different types of abdominal organs/tissue and the pancreatic tumor images, which reflected the characteristics of iopamidol and Fenestra VC, were obtained by micro-CT scanning. In living animals, iopamidol clearly enhanced the visibility of major abdominal organs/tissue parenchyma, and simultaneously the kidneys and urinary tract were prominently contrasted and the radial white linear artifacts were seen in the regions. However, the contrasts among organs/tissue were thought to be attenuated by renal excretion during micro-CT scanning. In a sacrificed animal, the parenchyma and the edge of pancreas and other organs/tissue were clearly visible and Ao and IVC were also visualized as compared with living animals. The artifacts by iopamidol which appeared in living animals were not observed in the sacrificed animals. Assessments of such contrast agents, which are excreted rapidly, by using sacrificed animals may also be useful in addition to using living animals. On the other hand, Fenestra VC predominantly increased the visibility of major abdominal vascular systems and was likely retained during micro-CT scanning for 40 min. Ford

abdominal organs in mice were retained for 24 h after injection of Fenestra VC. The present study also supported the benefits of Fenestra VC to vascular systems imaging when scanning for longer periods of time.

Most pancreatic tumor imaging with contrast agents such as nonionic iodine materials including iopamidol typically appeared as a hypoattenuating mass relative to the pancreatic parenchyma in humans.[19] The same is true with the case of BOP-treated hamsters. However the contrast between tumors and parenchyma in hamster pancreas was slightly inferior to that in humans, despite the higher dose of iopamidol than the manufacturer's recommendations for humans. It is implied that the difference in effects of nonionic contrast agents on humans and hamsters is the rapid clearance of iopamidol during image scanning, resulting in attenuation of the contrast of pancreatic parenchyma. From the viewpoint of toxicological effects of such contrast agents, repeated intravenous administrations of iopamidol for 5 weeks in rats at a dose of 2 g/kg BW iodine equivalent, which is almost similar to the present dose (1.85 g/kg BW iodine equivalent), did not show remarkable influences on body weights, food intakes, and hematological parameters (manufacturer's in-house data). Therefore, it is likely that the present doses of each agent under the Isoflurane anesthesia with the use of respiratory gating systems might be safe in single or short-term repeated administration studies. However, the influence of repeated treatment with iopamidol on general toxicities and pancreatic carcinogenesis in hamsters is still unclear. Further detailed analyses are be required to elucidate these points. Baron reported that differences of at least 10–15 CT value (HU; Hounsfield unit) are required for visual detection of the tumor.[20] In other words, higher contrasts between tumor and parenchyma images by micro-CT are required for differentiating histomorphological changes in the tumors as compared with pancreatic parenchyma. In the present study, all the tumors observed by micro-CT were histopathologically diagnosed as pancreatic ductal carcinomas, which are also the frequently observed pancreatic carcinoma type in humans.

BOP-induced pancreatic tumors over 4 mm in diameter. However, carcinoma-localized intralobules were not fully detected by micro-CT. The reason for this might also be due to insufficient contrast between the pancreatic tumor and parenchyma. Recently, Hainfeld *et al.*[21] reported that gold nanoparticles with higher X-ray absorptive power than iodine-based agents may be useful as a novel X-ray contrast agent. Further studies using powerful X-ray absorptive agents may shed light on the limitations of imaging with smaller sized pancreatic tumors. For evaluations of novel contrast agents, X-ray micro-CT imaging systems with BOP-induced pancreatic carcinogenesis models could be adequate.

In the present study, we focused on the imaging of both pancreatic morphology and BOP-induced pancreatic tumors at one time point using two types of contrast agents. Time-dependent imaging of pancreatic tumors might also be useful for evaluations of the tumor development and preventives for pancreatic carcinogenesis. Overall, iopamidol could clearly contrast between pancreatic parenchyma and the tumors as compared with Fenestra VC.

In conclusion, our results provided evidence that respiratory-gated micro-CT scanning of hamsters has potential as a method for evaluating changes in the growth of pancreatic tumors. These studies on scanning and pancreatic carcinogenesis model systems may also be useful for evaluation of newly developing contrast agents for pancreatic tumors. Development of novel contrast agents in combination with the improvement of devices may lead to detection of smaller pancreatic tumors and precancerous lesions.

Acknowledgments

This work was supported by Grants-in-Aid for Cancer Research, for the Third-Term Comprehensive 10-Year Strategy for Cancer Control, from the Ministry of Health, Labour and Welfare of Japan.

References

1 Matsuda T, Marugame T, Kamo K, Katanoda K, Ajiki W, Sobue T. Cancer incidence and incidence rates in Japan in 2002: based on data from 11 population-based cancer registries. *Jpn J Clin Oncol* 2008; **38**: 641–8.
2 Michaud DS. Epidemiology of pancreatic cancer. *Minerva Chir* 2004; **59**: 99–111.
3 Tsukuma H, Ajiki W, Ioka A, Oshima A. Survival of cancer patients diagnosed between 1993 and 1996: a collaborative study of population-based cancer registries in Japan. *Jpn J Clin Oncol* 2006; **36**: 602–7.
4 de Braud F, Cascinu S, Gatta G. Cancer of pancreas. *Crit Rev Oncol Hematol* 2004; **50**: 147–55.
5 Agarwal B, Correa AM, Ho L. Survival in pancreatic carcinoma based on tumor size. *Pancreas* 2008; **36**: e15–20.
6 Pongprasobchai S, Pannala R, Smyrk TC *et al.* Long-term survival and prognostic indicators in small (<or=2 cm) pancreatic cancer. *Pancreatology* 2008; **8**: 587–92.
7 Freeny PC, Marks WM, Ryan JA, Traverso LW. Pancreatic ductal adenocarcinoma: diagnosis and staging with dynamic CT. *Radiology* 1988; **166**: 125–33.
8 Legmann P, Vignaux O, Dousset B *et al.* Pancreatic tumors: comparison of dual-phase helical CT and endoscopic sonography. *AJR Am J Roentgenol* 1998; **170**: 1315–22.
9 Prokesch RW, Schima W, Chow LC, Jeffrey RB. Multidetector CT of pancreatic adenocarcinoma: diagnostic advances and therapeutic relevance. *Eur Radiol* 2003; **13**: 2147–54.
10 Bronstein YL, Loyer EM, Kaur H *et al.* Detection of small pancreatic tumors with multiphasic helical CT. *AJR Am J Roentgenol* 2004; **182**: 619–23.
11 Cavanaugh D, Johnson E, Price RE, Kurie J, Travis EL, Cody DD. In vivo respiratory-gated micro-CT imaging in small-animal oncology models. *Mol Imaging* 2004; **3**: 55–62.
12 Li XF, Zanzonico P, Ling CC, O'Donoghue J. Visualization of experimental lung and bone metastases in live nude mice by X-ray micro-computed tomography. *Technol Cancer Res Treat* 2006; **5**: 147–55.
13 Hori Y, Takasuka N, Mutoh M *et al.* Periodic analysis of urethane-induced pulmonary tumors in living A/J mice by respiration-gated X-ray microcomputed tomography. *Cancer Sci* 2008; **99**: 1774–7.
14 Bakan DA, Weichert JP, Longino MA *et al.* Polyiodinated triglyceride lipid emulsions for use as hepatoselective contrast agents in CT: effects of physicochemical properties on biodistribution and imaging profiles. *Invest Radiol* 2000; **35**: 158–69.
15 Konishi Y, Mizumoto K, Kitazawa S, Tsujiuchi T, Tsutsumi M, Kamano T. Early ductal lesions of pancreatic carcinogenesis in animals and humans. *Int J Pancreatol* 1990; **7**: 83–9.
16 Pour P, Althoff J, Kruger FW, Mohr U. A potent pancreatic carcinogen in Syrian hamsters: *N*-nitrosobis(2-oxopropyl)amine. *J Natl Cancer Inst* 1977; **58**: 1449–53.
17 Mizumoto K, Tsutsumi M, Denda A, Konishi Y. Rapid production of pancreatic carcinoma by initiation with *N*-nitroso-bis(2-oxopropyl)amine and repeated augmentation pressure in hamsters. *J Natl Cancer Inst* 1988; **80**: 1564–7.
18 Ford NL, Graham KC, Groom AC, Macdonald IC, Chambers AF, Holdsworth DW. Time-course characterization of the computed tomography contrast enhancement of an iodinated blood-pool contrast agent in mice using a volumetric flat-panel equipped computed tomography scanner. *Invest Radiol* 2006; **41**: 384–90.
19 Prokesch RW, Chow LC, Beaulieu CF, Bammer R, Jeffrey RB Jr. Isoattenuating pancreatic adenocarcinoma at multi-detector row CT: secondary signs. *Radiology* 2002; **224**: 764–8.
20 Baron RL. Understanding and optimizing use of contrast material for CT of the liver. *AJR Am J Roentgenol* 1994; **163**: 323–31.
21 Hainfeld JF, Slatkin DN, Focella TM, Smilowitz HM. Gold nanoparticles: a new X-ray contrast agent. *Br J Radiol* 2006; **79**: 248–53.

doi: 10.1111/j.1349-7006.2010.01588.x

Novel immunohistochemical marker, integrin $\alpha_V\beta_3$, for BOP-induced early lesions in hamster pancreatic ductal carcinogenesis

TSUKASA KITAHASHI[1], MITSUYOSHI YOSHIMOTO[2] and TOSHIO IMAI[1]

[1]Central Animal Laboratory and [2]Cancer Prevention Basic Research Project, National Cancer Center Research Institute, Tokyo 104-0045, Japan

Received September 29, 2010; Accepted December 28, 2010

DOI: 10.3892/ol.2011.252

Abstract. *N*-nitrosobis(2-oxopropyl)amine (BOP)-induced pancreatic ductal carcinomas and early ductal lesions in Syrian hamsters have been reported to show histopathological resemblance to those in humans. Specific protein expression profiles have been found in human carcinomas, but a detailed molecular approach regarding the dissection of BOP-induced pancreatic carcinogenesis has yet to be determined. The present immunohistochemical study of early and advanced hamster lesions focused on five proteins reported to be overexpressed in human patients, to clarify interspecies phenotype similarity. Integrin $\alpha_V\beta_3$ was found to be overexpressed in the epithelial cells of 13 of 14 atypical hyperplasias and 6 of 6 adenocarcinomas. This overexpression was more frequent than in the remaining four proteins. However, immunoreactivity for α-enolase in epithelial cells and for kallikrein 7 and galectin-1/3 in both epithelial and stromal cells was also evident at various frequencies. Thus, similarities of tumor-associated protein expression between human and hamster pancreatic ductal lesions were confirmed, and integrin $\alpha_V\beta_3$ was identified as a potentially useful immunohistochemical marker for early lesions in hamsters.

Introduction

Pancreatic cancer is among the 10 most frequently occurring type of cancer. In Japan, pancreatic cancer is ranked fifth as a cause of cancer-related mortality. The mortality rate associated with this type of cancer also ranks high in other developed countries (1,2). The detection of pancreatic cancer at early operable stages is difficult, combined with the lack of curative treatment approaches other than complete surgical removal; thus, 5-year relative survival rates are less than 6% (3,4). Therefore, it is crucial to develop new diagnostic and preventive methods to complement any improvements in therapeutic methods for the reduction of mortality and morbidity, and to explore specific proteins overexpressed in early lesions during pancreatic carcinogenesis.

Specific protein expression profiles revealed by immunohistochemical and proteomic analyses are currently employed in the application of individualized therapy of advanced human pancreatic carcinomas (5-8). Consequently, a number of candidates of prognostic and/or predictive markers have been established (9,10). Examples expressed in early lesions show potential for the development of novel diagnostic and preventive strategies.

Chemically induced and transgenic animal models for pancreatic ductal carcinogenesis have been the target of investigation of the impact of environmental factors and the role of specific gene alterations in multistage carcinogenesis (11-15). Among the models established thus far, the *N*-nitrosobis(2-oxopropyl)amine (BOP)-induced hamster model is the first and most widely utilized based on similarities to human diseases in the morphological characteristics of, not only advanced cancers, but also early ductal lesions, as well as pivotal genetic alterations, including *K-ras* and *p16* (13,16-18). In particular, it is anticipated that molecular profiles are equivalent in the early stages. Although changes in the protein expression have been reported (5-8) in pancreatic carcinomas in humans, molecular details of BOP-induced pancreatic early lesions in hamsters have yet to be investigated. In the present study, an immunohistochemical analysis was conducted on pancreatic carcinomas and early lesions induced in BOP-treated hamsters, focusing on proteins already reported to be altered in human cases. As a result, integrin $\alpha_V\beta_3$ was found to be more frequently expressed in both pancreatic carcinomas and its precursors than the four remaining proteins investigated. The results obtained showed multiple similarities in tumor-associated protein expression between human and hamster pancreatic ductal lesions.

Materials and methods

Animals. A total of 12 female Syrian golden hamsters at 5 weeks of age were purchased from Japan SLC (Shizuoka, Japan). The animals were housed 3 to a plastic cage with soft woodchip bedding (Japan SLC) in an air-conditioned animal room maintained at 22±2˚C and 60±5% relative humidity, with

Correspondence to: Dr Toshio Imai, Central Animal Laboratory, National Cancer Center Research Institute, 5-1-1 Tsukiji, Chuo-ku, Tokyo 104-0045, Japan
E-mail: toimai@ncc.go.jp

Abbreviations: BOP, *N*-nitrosobis(2-oxopropyl)amine

Key words: integrin $\alpha_V\beta_3$, Syrian hamster, pancreatic ductal carcinoma, early stage, *N*-nitrosobis(2-oxopropyl)amine

Table I. Antibodies and antigen retrieval methods for immunochemistry.

Protein	Antibodies	Antigen retrieval
Integrin $\alpha_v\beta_3$	Anti-human integrin $\alpha_v\beta_3$ monoclonal (Clone LM609; Chemicon International, Temecula, CA, USA)	Autoclaved for 10 min at 121˚C in 10 mM Tris-HCl buffer, including 1 mM EDTA (pH 9.0)
Kallikrein 7	Anti-kallikrein 7 goat polyclonal (R&D Systems, Minneapolis, MN, USA)	Autoclaved for 10 min at 121˚C in 10 mM citrate buffer (pH 6.0)
Galectin 1	Anti-galectin-1 rabbit polyclonal (Protein Tech Group, Chicago, IL, USA)	Autoclaved for 15 min at 121˚C in 10 mM citrate buffer (pH 6.0)
Galectin 3	Anti-galectin-3 rabbit polyclonal (Santa Cruz Biotechnology, Santa Cruz, CA, USA)	Autoclaved for 10 min at 121˚C in 10 mM citrate buffer (pH 6.0)
α-Enolase	Anti-α-enolase rabbit polyclonal (Aviva Systems Biology LLC., San Diego, CA, USA)	Autoclaved for 10 min at 121˚C in distilled water

a 12:12 h light:dark cycle. A basal diet (CE-2; CLEA Japan, Tokyo, Japan) and water were available *ad libitum* throughout the experiment.

Treatment for pancreatic tumor induction. Following an acclimatization period of 1 week, 9 hamsters were subcutaneously injected with BOP (Nacalai Tesque, Kyoto, Japan) in saline at 10 mg/kg body weight every other day for a total of four times. Additionally, 3 hamsters treated with saline were maintained as control animals. The experimental protocols were approved by the Committee for Ethics of Animal Experimentation of the National Cancer Center and were carried out according to the Guidelines for Animal Experiments.

Histopathological examination. At 23 weeks of age, all 12 hamsters were sacrificed and each pancreas was removed, fixed in 10% buffered formalin, processed for embedding in paraffin, sectioned and stained with hematoxylin and eosin for histopathological evaluation. Pancreatic ductal proliferative lesions were classified as atypical hyperplasias (AHs) and adenocarcinomas (ACs) according to the criteria previously described (19). Briefly, AH consisted of ductules with increased cell proliferation but minimal nuclear atypia and no loss of polarity. The typical AC had a distinct tubular, cribriform or anaplastic pattern with severely atypical columnar or cuboidal epithelia.

Immunohistochemical staining. A total of five target proteins, known to be specifically expressed in pancreatic carcinoma tissues or cell lines established from pancreatic carcinomas, were selected, as previously reported (5-8). Antibodies and antigen retrieval methods used in this study are listed in Table I. The role played by each was: integrin $\alpha_v\beta_3$, a transmembrane glycoprotein, is involved in cell-to-cell and cell-to-matrix interactions and thus may contribute to cancer progression, invasiveness and metastasis (5); kallikrein 7, a member of the serine protease family, enhances pancreatic cancer cell invasion by shedding E-cadherin (6); galectin-1, a soluble β-galactoside-binding animal lectin, modulates cell adherence and plays a role in tumor progression (7); galectin-3, another soluble β-galactoside-binding animal lectin, modulates cell adherence (8); and α-enolase, a glycolytic enzyme, is involved in the conversion of 2-phosphoglycerate phosphoenolpyruvate (7,20). The streptavidin-biotin-peroxidase complex method (StreptABComplex/HRP; DakoCytomation, Glostrup, Denmark) was employed to determine the expression and localization of each protein, and the sections were lightly counterstained with hematoxylin for microscopic examination. Negative controls without primary antibody reactions were set for each protein using serial sections. The staining intensity of each protein was analyzed with reference to the positivity rate in all epithelial and stromal cells in AHs and ACs and represented as <10%, negative (-); 10-70%, moderately positive (+); and >70%, strongly positive (++).

Results

Pancreatic ductal lesions induced by BOP. A total of 14 AHs and 6 ACs were induced in the 9 hamsters treated with BOP, whereas no lesions were found in the 3 animals without carcinogen exposure. The incidences and multiplicities (mean ± SD) of AHs and ACs were 89%, 1.6±1.1 and 44%, 0.7±0.9, respectively. Only 1 case of AC showed poorly differentiated characteristics, while the remaining cases were moderately differentiated tubular ACs. All cases harbored abundant stroma (data not shown).

Immunohistochemical findings for the five proteins analyzed

Normal pancreas (Fig. 1). Pancreatic ductal and ductular cells as well as islet cells showed weak immunohistochemical staining for α-enolase in hamsters without BOP treatment. The reactions in ductal and islet cells were cytoplasmic and essentially homogeneous. Integrin $\alpha_v\beta_3$, kallikrein 7 and galectin 1/3 were almost negative in the normal pancreatic tissues.

Atypical hyperplasias (Fig. 2). Integrin $\alpha_v\beta_3$ and α-enolase were expressed predominantly in the epithelial components of AHs, whereas kallikrein 7 and galectin 1/3 were expressed in both the epithelial and adjacent stromal elements. The morphological characteristics of the numerous stromal cells positive for kallikrein 7 and/or galectin 1/3 characterized these cells as fibroblasts. Regarding subcellular staining, integrin $\alpha_v\beta_3$ was mostly localized in the cell cytoplasm, while appearing to aggregate with a granular pattern towards the apex from the nuclei in the epithelial cells. Concerning

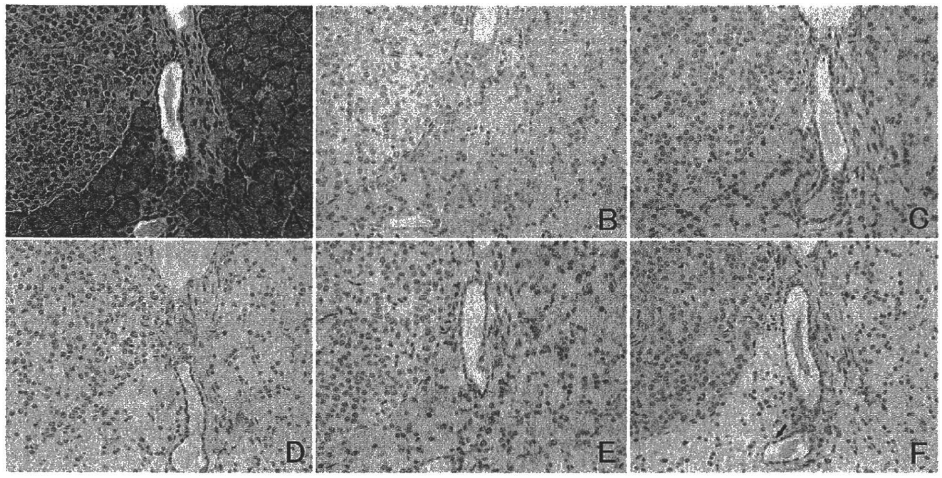

Figure 1. Normal hamster pancreatic tissue, including ductules (center panels), an islet (left panels) and acini (right panels). (A) H&E and immunohistochemistry for (B) integrin $\alpha_v\beta_3$, (C) kallikrein 7, (D) galectin 1, (E) galectin 3 and (F) α-enolase. The proteins were essentially negative, except for weak cytoplasmic positivity for (F) α-enolase in the islet and ductular cells (arrow). Original magnification, x200.

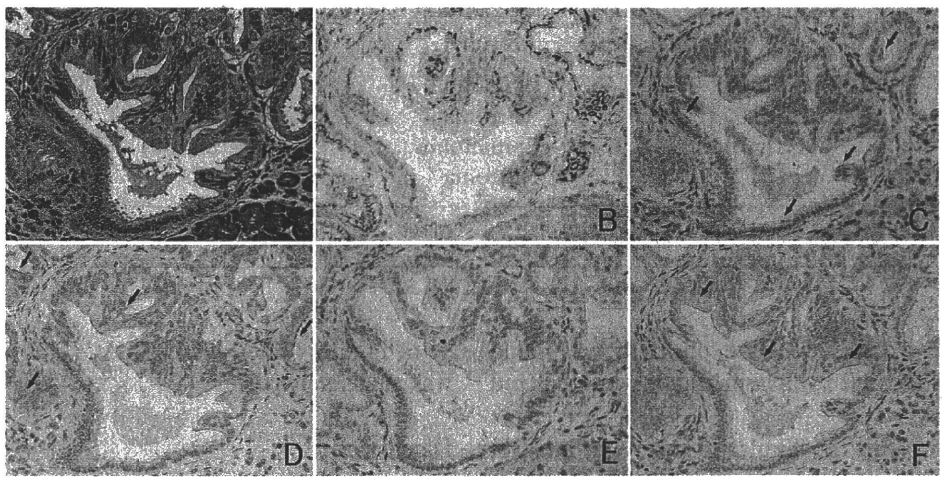

Figure 2. Atypical hyperplasia in a BOP-treated hamster. (A) H&E and immunohistochemistry for (B) integrin $\alpha_v\beta_3$, (C) kallikrein 7, (D) galectin 1, (E) galectin 3 and (F) α-enolase. (B) Integrin $\alpha_v\beta_3$ localization, particularly in the cytoplasm, with a granular pattern in the epithelial cells. In this case, (E) galectin 3 appears negative. (C, D and F) Other proteins are almost uniformly positive in the epithelial cytoplasm and/or are localized on the apical surface (arrows). Original magnification, x200.

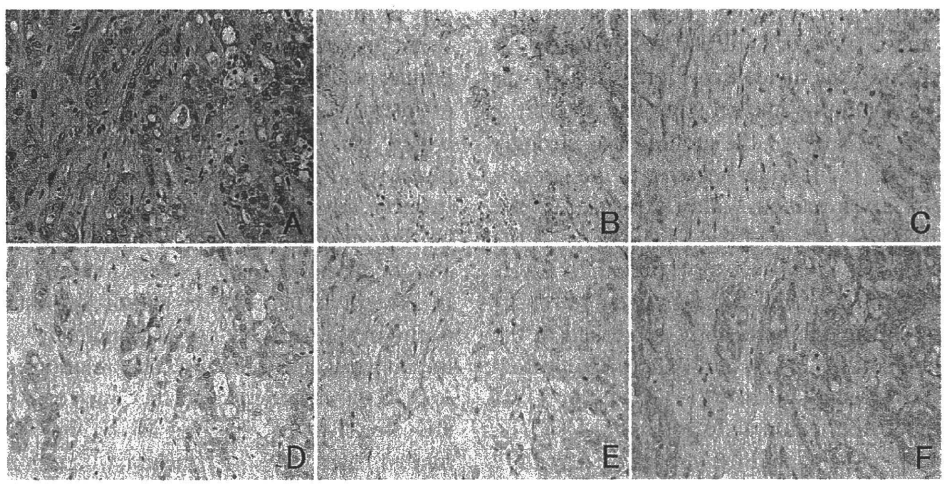

Figure 3. Adenocarcinoma in a BOP-treated hamster. (A) H&E and immunohistochemistry for (B) integrin $\alpha_v\beta_3$, (C) kallikrein 7, (D) galectin 1, (E) galectin 3 and (F) α-enolase. (B, D and F) Integrin $\alpha_v\beta_3$, galectin 1 and α-enolase are mainly positive in the epithelial tumor cells, and (C and E) kallikrein 7 and galectin 3 are mainly reactive in the stromal cells. Original magnification, x200.

Table II. Incidences and intensities of immunostaining in positive AHs and ACs.

Protein	Lesion	Location	Incidence (%)	
			Intensity (+)	Intensity (++)
Integrin $\alpha_V\beta_3$	AH (n=14)	Epithelium	8 (57)	5 (36)
		Stroma	0	0
	AC (n=6)	Epithelium	4 (67)	2 (33)
		Stroma	0	0
Kallikrein 7	AH (n=14)	Epithelium	6 (43)	0
		Stroma	4 (28)	4 (28)
	AC (n=6)	Epithelium	4 (66)	0
		Stroma	0	6 (100)
Galectin 1	AH (n=14)	Epithelium	0	3 (21)
		Stroma	1 (7)	0
	AC (n=6)	Epithelium	4 (67)	0
		Stroma	1 (17)	0
Galectin 3	AH (n=14)	Epithelium	2 (14)	1 (7)
		Stroma	1 (7)	1 (7)
	AC (n=6)	Epithelium	0	0
		Stroma	2 (33)	0
α-Enolase	AH (n=14)	Epithelium	11 (79)	0
		Stroma	0	0
	AC (n=6)	Epithelium	6 (100)	0
		Stroma	0	0

AH, atypical hyperplasia; AC, adenocarcinoma; +, moderately positive; ++, strongly positive.

kallikrein 7, galectin 1/3 and α-enolase, positivity was found almost uniformly in the cell cytoplasm and/or was localized on the apical surfaces.

Adenocarcinomas (Fig. 3). Similar to the AHs, integrin $\alpha_V\beta_3$ and α-enolase proved to be positive in the epithelia, while kallikrein 7 and galectin 1 were observed in the epithelial and stromal cells. Galectin 3 was stained only in the stromal cells. Subcellular staining patterns were similar to those in AHs.

Immunostaining incidences and intensities for the five proteins. Staining incidences and intensities for each protein were evaluated based on the positivity rates for cells (Table II). A total of 13 of14 AHs (93%) and 6 of 6 ACs (100%) were positive for integrin $\alpha_V\beta_3$. Consequently, the incidence of integrin $\alpha_V\beta_3$ was higher compared to the remaining four proteins, and in 5 of the AHs (36%) and 2 of the ACs (33%), the grading was strongly positive (++). Staining was found to be negative in the stroma. By contrast, kallikrein 7 was predominantly expressed in the stroma of 8 of 14 AHs (57%) and 6 of 6 ACs (100%), and the epithelial cells of 6 of 14 AHs (43%) were also stained. In 4 AHs (28%) and 6 ACs (100%), stromal cells were graded as strongly positive (++). Galectin 1 was predominantly expressed in the epithelium of 3 of 14 AHs (21%) and 4 of 6 ACs (67%), and all the AHs were graded as strongly positive (++). Galectin 3 was also expressed in both the epithelium and stroma of AHs (3/14, 21% and 2/14, 14%, respectively), and the stroma of ACs (2/6, 33%). Among the positive cases, 1 AH case showed strongly positive in both the epithelial and stroma cells. Expression of α-enolase was observed predominantly in the epithelial cells of 11 of 14 AHs (79%) and 6 of 6 ACs (100%). Staining intensity was moderately positive (+).

Discussion

The present immunohistochemical analysis focusing on five proteins reported to be overexpressed in human pancreatic carcinomas showed that integrin $\alpha_V\beta_3$ was found to be frequently and strongly expressed in BOP-induced hamster pancreatic early ductal lesions and carcinomas. This expression is in agreement with its reported promotion of cell migration and proliferation (21,22). Subcellular localization aggregated in the cytoplasm of epithelial cells has also been reported in human pancreatic cancer cases (5). Although a slight expression of integrin $\alpha_V\beta_3$ was found in pancreatic ductal hyperplasias, which lack cellular atypia and are thought to be initial histological focal changes, the frequency was lower than that in more advanced lesions (data not shown). The significance of the overexpression of integrin $\alpha_V\beta_3$ in pancreatic ductal carcinogenesis has yet to be elucidated. However, dysregulation in protein transportation and/or degradation functions may occur in the early stages of pancreatic ductal carcinogenesis in hamsters and humans. The relationship between integrin $\alpha_V\beta_3$-positivity and parameters, such as proliferation, apoptosis and invasiveness, has yet to be investigated. However, in human cases, 58% of pancreatic carcinomas showed positive staining and the frequency was significantly higher in primary tumors with lymph node metastasis (5). Recently, integrin $\alpha_V\beta_3$ was also studied as a target molecule for imaging diagnosis

in mammary carcinoma (23), and this BOP-induced hamster model may aid in the pre-clinical screening of integrin $\alpha_V\beta_3$ and other molecular-targeted probes and/or medicines.

Kallikrein 7 is a chymotrypsin-like serine protease, originally purified from human skin, which is specifically expressed in keratinizing squamous epithelia (24), and is involved in cell invasion by cleavage of the extracellular domain of adhesion molecules, such as E-cadherin. In the present study, Kallikrein 7 was found to be predominantly expressed in stromal cells of both AHs and ACs. Moderate-to-intense staining for kallikrein 7 has been reported in the majority of human pancreatic carcinomas, but this staining is distributed among the majority of the tumor cells (6). Although the cause of such variation remains to be determined, cytoplasmic positivity and/or localization on the apical surfaces was evident in the epithelial cells of some of our AHs and ACs in hamsters.

Galectin 1/3 are members of the family of β-galactoside-binding animal lectins (25) and play a role in a variety of cell functions, including proliferation, migration and adhesion characteristics (26,27). In this study, the expression of galectin 1/3 was observed at lower frequencies than the remaining three proteins in the epithelial and stromal cells in AHs, whereas it was strongly expressed in epithelial and stromal cells, respectively, in ACs. In human carcinoma cases, however, the opposite phenomenon has been described, with galectin 1 being stronger in the stroma and galectin 3 in the epithelial elements (7,8). The causes for this phenomenon remain to be determined.

α-Enolase, a glycolytic enzyme, is involved in the conversion of 2-phosphoglycerate to phosphoenolpyruvate in the glycolytic pathway (28). In the present analysis, α-enolase showed the second most frequent expression in the epithelium of both AHs and ACs. On the other hand, normal hamster pancreatic islets and acinar and ductal epithelium cells were weakly positive, partially consistent with a previous report (29).

In conclusion, some similarities to the human tumor-associated protein expression were confirmed in hamster pancreatic ductal lesions. The addition of molecules may also be identified by a global analysis using cDNA microarrays and/or proteomic approaches. Additional studies using hamsters may allow for the discovery of target molecules for practical diagnostic and preventive methods for human early pancreatic carcinomas.

Acknowledgements

This study was supported by Grants-in-Aid for the Third-Term Comprehensive Control Research for Cancer from the Ministry of Health, Labour and Welfare of Japan. We thank Dr Malcolm A. Moore for the revision of the scientific English language.

References

1. Matsuda T, Marugame T, Kamo K, Katanoda K, Ajiki W, Sobue T and the Japanese Cancer Surveillance Research Group: Cancer incidence and incidence rates in Japan in 2002: based on data from 11 population-based cancer registries. Jpn J Clin Oncol 38: 641-648, 2008.
2. Michaud DS: Epidemiology of pancreatic cancer. Minerva Chir 59: 99-111, 2004.
3. Tsukuma H, Ajiki W, Ioka A and Oshima A: Survival of cancer patients diagnosed between 1993 and 1996: a collaborative study of population-based cancer registries in Japan. Jpn J Clin Oncol 36: 602-607, 2006.
4. De Braud F, Cascinu S and Gatta G: Cancer of pancreas. Crit Rev Oncol Hematol 50: 147-155, 2004.
5. Hosotani R, Kawaguchi M, Masui T, Koshiba T, Ida J, Fujimoto K, Wada M, Doi R and Imamura M: Expression of integrin $\alpha_V\beta_3$ in pancreatic carcinoma: relation to MMP-2 activation and lymph node metastasis. Pancreas 25: e30-e35, 2002.
6. Johnson SK, Ramani VC, Hennings L and Haun RS: Kallikrein 7 enhances pancreatic cancer cell invasion by shedding E-cadherin. Cancer 109: 1811-1820, 2007.
7. Shen J, Person MD, Zhu J, Abbruzzese JL and Li D: Protein expression profiles in pancreatic adenocarcinoma compared with normal pancreatic tissue and tissue affected by pancreatitis as detected by two-dimensional gel electrophoresis and mass spectrometry. Cancer Res 64: 9018-9026, 2004.
8. Shimamura T, Sakamoto M, Ino Y, Shimada K, Kosuge T, Sato Y, Tanaka K, Sekihara H and Hirohashi S: Clinicopathological significance of galectin-3 expression in ductal adenocarcinoma of the pancreas. Clin Cancer Res 8: 2570-2575, 2002.
9. Gold DV, Modrak DE, Ying Z, Cardillo TM, Sharkey RM and Goldenberg DM: New MUC1 serum immunoassay differentiates pancreatic cancer from pancreatitis. J Clin Oncol 24: 252-258, 2006.
10. Takayama R, Nakagawa H, Sawaki A, Mizuno N, Kawai H, Tajika M, Yatabe Y, Matsuo K, Uehara R, Ono K, Nakamura Y and Yamao K: Serum tumor antigen REG4 as a diagnostic biomarker in pancreatic ductal adenocarcinoma. J Gastroenterol 45: 52-59, 2010.
11. Rivera JA, Graeme-Cook F, Werner J, Z'graggen K, Rustgi AK, Rattner DW, Warshaw AL and Fernández-del Castillo C: A rat model of pancreatic ductal adenocarcinoma: targeting chemical carcinogens. Surgery 122: 82-90, 1997.
12. Osvaldt AB, Wendt LR, Bersch VP, de Cássia A, Schumacher R, Edelweiss MI and Rohde L: Pancreatic intraepithelial neoplasia and ductal adenocarcinoma induced by DMBA in mice. Surgery 140: 803-809, 2006.
13. Pour P, Althoff J, Kruger FW and Mohr U: A potent pancreatic carcinogen in Syrian hamsters: *N*-nitrosobis(2-oxopropyl)amine. J Natl Cancer Inst 58: 1449-1453, 1977.
14. Hingorani SR, Petricoin EF, Maitra A, *et al*: Preinvasive and invasive ductal pancreatic cancer and its early detection in the mouse. Cancer Cell 4: 437-450, 2003.
15. Ueda S, Fukamachi K, Matsuoka Y, Takasuka N, Takeshita F, Naito A, Iigo M, Alexander DB, Moore MA, Saito I, Ochiya T and Tsuda H: Ductal origin of pancreatic adenocarcinomas induced by conditional activation of a human Ha-*ras* oncogene in rat pancreas. Carcinogenesis 27: 2497-2510, 2006.
16. Fujii H, Egami H, Chaney W, Pour P and Pelling J: Pancreatic ductal adenocarcinomas induced in Syrian hamsters by *N*-nitrosobis(2-oxopropyl)amine contain a c-Ki-*ras* oncogene with a point-mutated codon 12. Mol Carcinog 3: 296-301, 1990.
17. Li J, Weghorst CM, Tsutsumi M, Poi MJ, Knobloch TJ, Casto BC, Melvin WS, Tsai MD and Muscarella P: Frequent $p16^{INK4A/CDKN2A}$ alterations in chemically induced Syrian golden hamster pancreatic tumors. Carcinogenesis 25: 263-268, 2004.
18. Tsujiuchi T, Sasaki Y, Kubozoe T, Konishi Y and Tsutsumi M: Alterations in the Fhit gene in pancreatic duct adenocarcinomas induced by *N*-nitrosobis(2-oxopropyl)amine in hamsters. Mol Carcinog 36: 60-66, 2003.
19. Konishi Y, Mizumoto K, Kitazawa S, Tsujiuchi T, Tsutsumi M and Kamano T: Early ductal lesions of pancreatic carcinogenesis in animals and humans. Int J Pancreatol 7: 83-89, 1990.
20. Roda O, Chiva C, Espuna G, Gabius H, Real FX, Navarro P and Andreu D: A proteomic approach to the identification of new tPA receptors in pancreatic cancer cells. Proteomics 6: S36-S41, 2006.
21. Carreiras F, Lehmann M, Sichel F, Marvaldi J, Gauduchon P and Le Talaer JY: Implication of the $\alpha_V\beta_3$ integrin in the adhesion of the ovarian-adenocarcinoma cell line IGROV1. Int J Cancer 63: 530-536, 1995.
22. Yokosaki Y, Monis H, Chen J and Sheppard D: Differential effects of the integrins $\alpha_9\beta_1$, $\alpha_V\beta_3$, and $\alpha_V\beta_6$ on cell proliferative responses to tenascin. Roles of the β subunit extracellular and cytoplasmic domains. J Biol Chem 271: 24144-24150, 1996.

23. Beer AJ, Niemeyer M, Carlsen J, Sarbia M, Nährig J, Watzlowik P, Wester HJ, Harbeck N and Schwaiger M: Patterns of $\alpha_V\beta_3$ expression in primary and metastatic human breast cancer as shown by ^{18}F-Galacto-RGD PET. J Nucl Med 49: 255-259, 2008.
24. Hansson L, Strömqvist M, Bäckman A, Wallbrandt P, Carlstein A and Egelrud T: Cloning, expression, and characterization of stratum corneum chymotryptic enzyme. A skin-specific human serine proteinase. J Biol Chem 269: 19420-19426, 1994.
25. Barondes SH, Castronovo V, Cooper DN, *et al*: Galectins: a family of animal β-galactoside-binding lectins. Cell 76: 597-598 1994.
26. Perillo, NL, Marcus ME and Baum LG: Galectins: Versatile modulators of cell adhesion, cell proliferation, and cell death. J Mol Med 76: 402-412, 1998.
27. Maeda N, Kawada N, Seki S, Ikeda K, Iwao H, Okuyama H, Hirabayashi J, Kasai K and Yoshizato K: Stimulation of proliferation of rat hepatic stellate cells by galectin-1 and galectin-3 through different intracellular signaling pathways. J Biol Chem 278: 18938-18944, 2003.
28. Zhou W, Capello M, Fredolini C, Piemonti L, Liotta LA, Novelli F and Petricoin EF: Mass spectrometry analysis of the post-translational modifications of α-enolase from pancreatic ductal adenocarcinoma cells. J Proteome Res 9: 2929-2936, 2010.
29. Ahmed M and Bergsten P: Glucose-induced changes of multiple mouse islet proteins analysed by two-dimensional gel electrophoresis and mass spectrometry. Diabetologia 48: 477-485, 2005.

Preventive Medicine 52 (2011) 227–233

Contents lists available at ScienceDirect

Preventive Medicine

journal homepage: www.elsevier.com/locate/ypmed

Leisure-time physical activity and breast cancer risk defined by estrogen and progesterone receptor status—The Japan Public Health Center-based Prospective Study

Reiko Suzuki [a], Motoki Iwasaki [a,*], Seiichiro Yamamoto [b], Manami Inoue [a], Shizuka Sasazuki [a], Norie Sawada [a], Taiki Yamaji [a], Taichi Shimazu [a], Shoichiro Tsugane [a] and The Japan Public Health Center-based Prospective Study Group

[a] Epidemiology and Prevention Division, Research Center for Cancer Prevention and Screening, National Cancer Center, 5-1-1 Tsukiji, Chuo-ku, Tokyo, 104–0045, Japan
[b] Cancer Information Services and Surveillance Division, Center for Cancer Control and Information Services, National Cancer Center, 5-1-1 Tsukiji, Chuo-ku, Tokyo, 104–0045, Japan

ARTICLE INFO

Available online 2 February 2011

Keywords:
Breast cancer
Estrogen receptor
Leisure-time physical activity
Metabolic equivalents
Progesterone receptor
Risk

ABSTRACT

Objective. The study aims to investigate the association between leisure-time physical activity and breast cancer risk in consideration of tumor estrogen-receptor/progesterone-receptor status.

Methods. We conducted a population-based prospective cohort study among 53,578 women in the Japan Public Health Center-based Prospective Study. Leisure-time physical activity was assessed by self-reported questionnaires. A Cox proportional hazards regression model was used to derive relative risks and 95% confidence intervals.

Results. From 1990–1993 to the end of 2007, 652 cases were identified. The breast cancer rates (per 100,000 person-years) in the sedentary groups (≤3 days/month) was 84 in overall, 97 in premenopausal and 75 in postmenopausal women. We observed a statistically significant inverse association between leisure-time physical activity and breast cancer risk (relative risk$_{\geq 3 \text{ days/week vs. } \leq 3 \text{ days/month}}$ = 0.73; 95% confidence interval 0.54–1.00; p_{trend} 0.037), particularly in estrogen receptor+progesterone receptor+ (relative risk 0.43; 0.19–1.00; p_{trend} 0.022), and this inverse trend was apparent among postmenopausal women (relative risk 0.25; 0.06–1.06; p_{trend} 0.041). An inverse trend was also observed between daily total physical activity and postmenopausal estrogen receptor+progesterone receptor+ risk (p = 0.046). Among body mass index ≥25 kg/m^2 group, leisure-time physical activity was associated with decreased risk (relative risk$_{\geq 1 \text{ day/week vs. } \leq 3 \text{ days/month}}$ = 0.65; 0.43–0.97; p_{trend} 0.033).

Conclusion. Active participation in leisure-time physical activity may contribute to a decrease in breast cancer risk, particularly for postmenopausal estrogen receptor+progesterone receptor+ tumors.

Introduction

The latest report of the World Cancer Research Fund (World Cancer Resarch Fund/American Institute for Cancer Resarch, 2007) states that physical activity (PA) probably contributes to a decrease in the risk of breast cancer. The biological mechanisms underlying this inverse association have yet to be confirmed but may partly include the decreased production or bioavailability of endogenous female hormones (McTiernan et al., 2004), or of metabolic-related hormones and growth factors, such as estrogens, insulin (Regensteiner et al., 1991) and insulin-like growth factors (Raastad et al., 2000), which may stimulate cellular proliferation/differentiation in the breast (Bernstein and Ross, 1993; Hankinson et al., 1998). Other proposed mechanisms include an improvement in immune function (Shephard et al., 1995).

Owing to the possible involvement of hormone-related mechanisms, the association has been evaluated with consideration to the estrogen- and progesterone-receptor (ER/PR) status of tumors (Adams et al., 2006; Bardia et al., 2006; Bernstein et al., 2005; Britton et al., 2002; Chlebowski et al., 2007; Dallal et al., 2007; Enger et al., 2000; Lee et al., 2001; Leitzmann et al., 2008; Peters et al., 2009; Schmidt et al., 2008). The majority of studies were conducted among Western populations, however, and the results have been inconsistent.

In Japan, the incidence rate of breast cancer has increased steeply over the last three decades, and this cancer is currently the most

Abbreviations: CIs, confidence intervals; BMI, body mass index; DTPA, daily total physical activity; EFH, exogenous female hormone; ER, estrogen receptor; PA, physical activity; PHC, public health center; PR, progesterone receptor; FFQ, food frequency questionnaire; LPA, leisure-time physical activity; METs, metabolic equivalents; RR, relative risk; SD, standard deviation.

* Corresponding author. Fax: +81 3 3547 8578.
E-mail address: moiwasak@ncc.go.jp (M. Iwasaki).

0091-7435/$ – see front matter © 2011 Elsevier Inc. All rights reserved.
doi:10.1016/j.ypmed.2011.01.016

common cancer (Matsuda et al., 2010). Among Asian populations, however, few epidemiological studies have prospectively evaluated the association in consideration of ER/PR (Suzuki et al., 2010).

We hypothesized that PA may be associated with a decreased risk of breast cancer partly through hormone-related mechanisms, on the basis that PA may lead to a decrease in body fat (Sternfeld et al., 2005), the main source of endogenous estrogen after menopause (Cleland et al., 1985). Here, we evaluated the association between PA and ER/PR-defined breast cancer risk in 53,578 Japanese women in the Japan Public Health Center-based Prospective Study (JPHC).

Methods

Study participants

The JPHC was launched in 1990 to evaluate the association between lifestyle factors, cancer, and cardiovascular disease among the Japanese population. Details have been provided elsewhere (Tsugane and Sobue, 2001). The target population was all Japanese residents aged 40–69 years enrolled in the residential registries of 11 public health centers (PHCs). Two cohorts were enrolled (cohort I, Iwate-Ninohe, Akita-Yokote, Nagano-Saku, Okinawa-Chubu, and Tokyo-Kastushika; and cohort II, Ibaraki-Mito, Niigata-Nagaoka, Kochi-Chuohigashi, Nagasaki-Kamigoto, Okinawa-Miyako, and Osaka-Suita). Initially, 71,698 women were invited. Kastushika (cohort I) could not be included due to a lack of information on cancer incidence ($n=4{,}178$). We excluded women who did not possess Japanese nationality, moved before the start of follow-up, were not aged 40–69 years, or who had duplicate data ($n=146$).

Of the remainder, 55,838 completed the baseline questionnaires (response rate 83%). All eligible subjects were sent 5-year (1995–1998; response rate 80%) and 10-year follow-up questionnaires (2000–2003; response rate 78%). We excluded women with a self-reported history of cancer before the start of follow-up ($n=1{,}509$). To investigate the impact of leisure-time physical activity (LPA) on breast cancer risk, we excluded women with missing information on LPA ($n=751$). Age-area-adjusted analysis was conducted in 53,578 women.

Further, we then excluded women who had missing or unreliable information on height, BMI, BMI at age 20 years (<14 or ≥40), alcohol intake, smoking, or use of exogenous female hormones (EFH) ($n=13{,}804$), as well as those with a family history of breast cancer ($n=210$) and women who reported unreasonable estimates of total energy intake (±3SD) ($n=395$). Finally, 39,169 women were included in multivariable-adjusted analysis. We also performed sub-analyses to evaluate the impact of daily total physical activity (DTPA) in cohort II only because baseline information on DTPA was available.

Exposure measurement

The main exposure of interest was participation frequency in LPA. We inquired about the frequency of participation in non-occupational LPA, such as sports and exercise, at the baseline and 5-year follow-up surveys. In both questionnaires, we asked 'How many times did you participate in sports and PA other than during working hours,' with five predefined categories of almost never exercise: 1–3 days per month, 1–2 days per week, 3–4 days per week, and almost daily.

In cohort II, we evaluated the impact of DTPA on breast cancer risk. DTPA was measured as metabolic equivalents (METs-hours/day). Calculation in METs has been explained elsewhere (Inoue et al., 2008). The same methods were used in the baseline and 5-year follow-up surveys because they contained common questions on sleeping time, heavy physical work or strenuous exercise, standing or walking time, and sitting time.

Although LPA was not directly validated, the validity and reproducibility of the total METs/day score for the 5-year follow-up questionnaire was previously evaluated using 4-day, 24-hour PA records as an objective standard in 108 volunteer subjects in the cohort. In brief, correlations between the 5-year follow-up questionnaire and 4-day, 24-h record showed reasonable validity, with a Spearman rank correlation coefficient of 0.35 in women (Inoue et al., 2008). Reproducibility for the 5-year follow-up questionnaire was also supported, with a Spearman rank correlation coefficient of 0.68 (Imai et al., 2010).

Ascertainment of cases and follow-up

Breast cancer cases were identified by active patient notification from major local hospitals and data linkage with population-based cancer registries, with permission from the local governments responsible for the registries. Cases were defined as codes C500–509 (World Health Organization, 2000). Diagnosis was microscopically verified for 97% of all case patients. ER/PR status was evaluated by either immunohistochemical assay or enzyme-linked immunoassay. The cut-off point for positive receptor status was defined by clinical estimation at the treating hospital or by the assay method of the clinical laboratory. In most but not all cases, hormone receptor-positivity was defined as the presence of ≥10 fmol/mg protein in enzyme-linked immunoassay or by the finding of any positive cells in a specimen in immunohistochemical assay.

Follow-up was started on the date of administration of the baseline questionnaire and continued until the date of diagnosis of breast cancer, date of death, date of moving, or end of follow-up (December 31, 2007), whichever occurred first. Date of death or moving was verified through linkage with the death or residential registry at the respective PHC.

Statistical analysis

We used time-dependent multivariable Cox proportional hazards regression models to evaluate relative risks (RRs) and 95% confidence intervals (CIs) using age as the time scale (Korn et al., 1997). Women were subdivided into three categories by LPA [≤3 days/month, 1–2 days/week, ≥3 days/week]. The multivariable adjusted model included height, recent BMI, BMI at age 20 years, smoking status, age at menarche, age at first birth, parity, age at menopause, use of EFH, alcohol intake and isoflavone intake. These factors were based on the self-administered baseline questionnaires and were updated with the follow-up surveys, if available. If they could not be properly adjusted due to the small number of ER/PR-defined cases, these covariates were excluded, as mentioned in the footnotes in Table 2. For DTPA, women were subdivided according to tertile. Trend tests were conducted by creating a continuous variable in the rank order of each category. Additional analyses were conducted with stratification by menopausal and BMI status. All analyses were performed using the SAS statistical package version 9.1 (SAS Institute, Cary, NC). All statistical tests were two-sided, and statistical significance was defined as $p<.05$.

Results

After an average 14.5 years of follow-up, 652 breast cancer cases were diagnosed among 53,578 women. Information on ER/PR status was available for 299, showing 135 cases of ER+PR+, 64 of ER+PR−, and 83 of ER−PR−. Although height and BMI did not appear to differ by LPA level, women who tended to participate were more likely to be older and not to use EFH (Table 1).

Overall, we observed a statistically significant inverse association between LPA and breast cancer risk [multivariable-adjusted $RR_{\geq 3\ days/week\ vs.\ \leq 3\ days/week}=0.73$; 95% CI 0.54–1.00; p_{trend} 0.038]. In particular, the observed inverse association was apparent for ER+PR+ tumors (corresponding $RR_{ER+PR+}=0.43$ (0.19–1.00) p_{trend} 0.022), but not for others (Table 2). Without updating exposure information (i.e. by using the baseline information only), the corresponding result for ER+PR+ was no longer statistically significant [0.64 (0.29–1.38) $p_{trend}=0.13$ (text only)], although the point estimates of RRs were less than 1 at either baseline alone or with updated information. Further analyses without adjustment of recent BMI or BMI at 20 years old gave similar results.

In analyses stratified by menopausal status, LPA participation was marginally inversely associated with overall breast cancer risk among premenopausal women, although null association was observed after considering ER/PR tumor status. Among postmenopausal women, in contrast, LPA was associated with a decreased risk of ER+PR+ tumors using repeated exposure information (i.e. both baseline and 5-year follow-up surveys) [multivariable-adjusted $RR_{\geq 3\ days/week\ vs.\ \leq 3\ days/month}=0.25$ (0.06–1.06) p_{trend} 0.041; Table 2].

Table 1
Subject characteristics according to category of participation in leisure-time activity in the Japan Public Health Center-based Prospective Study (1990/1993–).

Characteristic	Frequency of participation in leisure-time physical activity		
	≤3 days/month	1–2 days/week	≥3 days/week
At baseline survey (%)	81.4	9.7	8.9
At 5-year follow-up survey (%)	78.1	10.8	11.2
Age at baseline survey, y, mean (SD)	51.1 (7.8)	50.5 (7.9)	54.2 (8.2)
Body mass index at age 20, kg/m^2, mean (SD)	21.5 (2.6)	21.2 (2.4)	21.6 (2.7)
Body mass index at baseline, kg/m^2, mean (SD)	23.3 (3.1)	23.2 (2.9)	23.5 (3.2)
Height, cm, mean (SD)	152.2 (5.4)	153.4 (5.3)	152.1 (5.7)
Age at menarche, y, mean (SD)	14.5 (1.8)	14.3 (1.8)	14.9 (1.9)
Age at first birth, y, mean (SD)[a]	24.9 (3.4)	25.1 (3.1)	25.0 (3.5)
Number of children, *n*, mean (SD)	2.6 (1.5)	2.6 (1.4)	2.7 (1.6)
Age at menopause, y, mean (SD)	48.3 (4.7)	48.4 (4.8)	48.7 (4.5)
Use of exogenous hormones at baseline (ever), %	12.6	12.5	11.7
Alcohol drinking status at baseline (ever), %	22.4	29.9	23.1
Smoking status at baseline (ever), %	8.0	7.6	7.2
Intake of isoflavones, mg, mean[b]	36.2	39.0	42.9

BMI = body mass index, SD = standard deviation.
[a] Based on information among parous women.
[b] Standardized according to food frequency questionnaires.

In cohort II, the impact of DTPA on breast cancer risk showed no overall association (multivariable-adjusted $RR_{\text{tertile3 vs. tertile1 METs/day score}} = 1.03$ (0.75–1.41) p_{trend} 0.86; Table 3). On consideration of menopausal and ER/PR status, however, we observed a substantial inverse trend between DTPA and ER+PR+ tumors among Postmenopausal women (age-area adjusted $RR_{\text{tertile3 vs. tertile1 METs/day score}} = 0.43$ (0.17–1.08) p_{trend} 0.046; Table 3).

On stratification by BMI (<25 or ≥25 kg/m^2), no association between LPA and breast cancer risk was seen among women with BMI <25 kg/m^2. Among overweight women (BMI ≥25 kg/m^2), however, participation in LPA was associated with a decreased risk of breast cancer risk overall ($RR_{\geq 1 \text{ day/week vs. } \leq 3 \text{ days/month}} = 0.65$ (0.43–0.97) p_{trend} 0.033; Table 4).

Discussion

This is the first large prospective cohort study to evaluate the association between LPA and breast cancer risk in consideration of ER/PR status in a Japanese population. Overall, LPA showed a substantial inverse association with breast cancer risk after adjustment for all covariates. Among premenopausal women, LPA was marginally associated with a decreased risk overall but not for specific ER/PR tumors. Among postmenopausal women, LPA was associated with a decreased risk for ER+PR+ tumors. Although there was no overall association between DTPA and breast cancer risk, we observed a considerable inverse trend between DTPA and postmenopausal ER+PR+ tumors in a JPHC sub-cohort. Further, on stratification by BMI, we observed a substantial inverse association between LPA and breast cancer risk among overweight women.

Our observed favorable impact of LPA against breast cancer risk was consistent with previous results for overall (Bardia et al., 2006) and ER+ tumors (Bernstein et al., 2005), although a cohort study suggested an inverse association for ER− but not ER+ tumors (Dallal et al., 2007).

Among premenopausal women, the marginal inverse trend of an association of LPA with breast cancer risk was found for overall tumors but not for any tumor subtypes. PA has been reported to exert a protective effect on risk for overall tumors (Maruti et al., 2008) and irrespective of hormone receptor positivity (Enger et al., 2000) (Adams et al., 2006) (Suzuki et al., 2010). The observed weak inverse trend might be due to the fact that our follow-up period did not cover the entire premenopausal period because follow-up started at around age 40.

Unlike previous results (McTiernan et al., 2003) (Lee et al., 2001), we found no inverse trend among postmenopausal women. For ER+PR+ tumors, however, a substantial inverse trend was found, in line with some (Chlebowski et al., 2007; Peters et al., 2009; Schmidt et al., 2008) but not all previous studies (Lee et al., 2001) (Leitzmann et al., 2008). A protective effect of PA on both ER+PR+ and ER+PR− tumors has also reported (Bardia et al., 2006).

Among overweight women, a substantial decreased in risk with LPA was observed overall. Similarly, a weak inverse trend was also observed for ER+PR+ tumors. In other studies, however, an inverse association was observed among a low-BMI group (Leitzmann et al., 2008), particularly for ER+PR+ tumors (Enger et al., 2000). These inconsistent results indicate the need for further careful evaluation.

Unlike LPA, our sub-analyses for DTPA (average 9.2 person-years of follow-up) did not show any overall favorable impact, which was consistent with our previous analysis with an average 7.5 person-years of follow-up (from 1995–1999 to 2004) (Inoue et al., 2008). In contrast, our corresponding present results for the postmenopausal ER+PR+ tumors showed a substantial inverse trend with DTPA. Although these results could not be clearly explained and might not exclude the possible involvement of non-hormone-related mechanisms, the observed results for postmenopausal ER+PR+ tumors might support the idea that PA is associated with a decreased risk of breast cancer partly through hormone-related mechanisms. After menopause, exercise may lead to a decrease in adipose tissue (Sternfeld et al., 2005), a major source of endogenous estrogen derived from the peripheral conversion of androgens to estrogens (Cleland et al., 1985) or to an increase in sex hormone-binding globulin (van Gils et al., 2009), the main protein carrier of estradiols, or both. A lack of association of DTPA with overall breast cancer risk in the present and a previous JPHC study (Inoue et al., 2008) might be explained without consideration of menopausal and ER/PR status. Further study with regard to menopausal status, ER/PR status or type of PA is required.

Strengths of our study include its prospective population-based cohort study design and large study size, adjustment for a broad range of potential confounders, and availability of repeated measurements for exposure as well as some covariates, which can change during long follow-up. Time-dependent analyses may reduce the misclassification of exposure and improve statistical efficiency. The study design, with a long follow-up period and repeated exposure measurements, might have aided detection of this inverse association.

Our main limitation was that ER/PR status was available for only about 46% of cases. The major reason for an unknown ER/PR status was likely that data collection began in 2002, while data during follow-up from 1990 to 2002 were obtained by retrospective review of medical records or pathology reports. Potential bias due to this relatively large number of cases with unknown ER/PR status should be

Table 2
Relative risks (RRs) and 95% confidence intervals (CIs) for the association between leisure-time activity and breast cancer risk among Japanese women in the Japan Public Health Center-based Prospective Study, 1990–2007.

Type of tumor	All					Premenopausal women[b]					Postmenopausal women[c]				
	Participation frequency in leisure-time physical activity					Participation frequency in leisure-time physical activity					Participation frequency in leisure-time physical activity				
		≤3 days/ month	1–2 days/ week	≥3 days/ week			≤3 days/ month	1–2 days/ week	≥3 days/ week			≤3 days/ month	1–2 days/ week	≥3 days/ week	
	Cases/*n*	Ref.	RR (95% CI)	RR (95% CI)	p_{trend}	Cases/*n*	Ref.	RR (95% CI)	RR (95% CI)	p_{trend}	Cases/*n*	Ref.	RR (95% CI)	RR (95% CI)	p_{trend}
Cases		529	59	64			254	25	21			275	34	43	
Total person-years		627669	73985	78439			260618	33986	24129			367051	39999	54310	
Model[a]	652/53,578	1.00 (ref.)	0.98 (0.75–1.29)	0.83 (0.64–1.08)	0.19	300/21,799	1.00 (ref.)	0.76 (0.50–1.15)	0.70 (0.45–1.10)	0.06	352/31,779	1.00 (ref.)	1.16 (0.81–1.66)	0.98 (0.71–1.36)	0.89
		389	45	45			200	23	17			189	22	28	
Model[d]	479/39,169	1.00 (ref.)	0.86 (0.63–1.18)	0.73 (0.54–1.00)	0.037	240/17,332	1.00 (ref.)	0.82 (0.53–1.27)	0.66 (0.40–1.09)	0.074	239/21837	1.00 (ref.)	0.88 (0.56–1.38)	0.78 (0.52–1.17)	0.21
ER+PR+		115	10	10			55	3	4			60	7	6	
Model[a]	135/53,578	1.00 (ref.)	0.83 (0.43–1.58)	0.61 (0.32–1.18)	0.12	62/21,799	1.00 (ref.)	0.48 (0.15–1.54)	0.61 (0.22–1.70)	0.19	73/31,779	1.00 (ref.)	1.13 (0.51–2.47)	0.67 (0.29–1.54)	0.44
		89	6	6			48	3	4			41	3	2	
Model[d]	101/39,169	1.00 (ref.)	0.55 (0.24–1.26)	0.43 (0.19–1.00)	0.022	55/17,332	1.00 (ref.)	0.54 (0.17–1.74)	0.64 (0.23–1.78)	0.25	46/21,837	1.00 (ref.)	0.62 (0.19–2.01)	0.25 (0.06–1.06)	0.041
ER+PR−		50	6	8			25	4	2			25	2	6	
Model[a]	64/53,578	1.00 (ref.)	1.21 (0.52–2.82)	1.18 (0.55–2.50)	0.60	31/21,799	1.00 (ref.)	1.45 (0.50–4.20)	0.73 (0.17–3.11)	0.91	33/31,779	1.00 (ref.)	0.83 (0.20–3.50)	1.60 (0.65–3.94)	0.37
		33	5	8			19	4	2			14	1	6	
Model[e]	46/39,169	1.00 (ref.)	1.28 (0.49–3.32)	1.93 (0.87–4.26)	0.11	25/17,332	1.00 (ref.)	2.04 (0.68–6.16)	0.90 (0.20–3.94)	0.74	21/21,837	1.00 (ref.)	0.56 (0.07–4.56)	3.12 (1.15–8.50)	0.049
ER−PR−		66	6	11			28	1	4			38	5	7	
Model[a]	83/53,578	1.00 (ref.)	0.91 (0.39–2.11)	1.30 (0.68–2.47)	0.51	33/21,799	1.00 (ref.)	0.34 (0.045–2.47)	1.35 (0.47–3.89)	0.92	50/31,779	1.00 (ref.)	1.35 (0.53–3.45)	1.34 (0.59–3.02)	0.41
		49	4	8			22	3				27	4	5	
Model[e]	61/39,169	1.00 (ref.)	0.67 (0.24–1.88)	1.06 (0.49–2.26)	0.92	25/17,332	1.00 (ref.)	0.55 (0.16–1.86)[f]		0.34	36/21,837	1.00 (ref.)	1.32 (0.46–3.82)	1.07 (0.41–2.82)	0.79
Unknown		285	35	33			137	15	9			148	20	24	
Model[a]	353/53,578	1.00 (ref.)	0.99 (0.70–1.42)	0.75 (0.52–1.07)	0.15	161/21,799	1.00 (ref.)	0.74 (0.43–1.28)	0.53 (0.27–1.04)	0.038	192/31,779	1.00 (ref.)	1.22 (0.76–1.95)	0.96 (0.62–1.48)	0.97
		210	28	22			104	14	7			106	14	15	
Model[d]	260/39,169	1.00 (ref.)	0.94 (0.63–1.40)	0.64 (0.41–1.00)	0.06	125/17,332	1.00 (ref.)	0.85 (0.48–1.51)	0.51 (0.23–1.10)	0.08	135/21,837	1.00 (ref.)	0.95 (0.54–1.67)	0.72 (0.41–1.24)	0.25

[a] Cox proportional hazards models was adjusted for age (time-scales) and area (10).
[b] For premenopausal women, multivariable Cox proportional hazards models were adjusted for all covariates (footnote d or e), except age at menopause.
[c] For postmenopausal women, multivariable Cox proportional hazards models were adjusted for all covariates (footnote d or e) and age at menopause (≤44, 45–54, ≥55 years).
[d] Multivariable Cox proportional hazards models were adjusted for age (time-scales), area (10), height (continuous), recent BMI (continuous), BMI at age 20 years (continuous), smoking status (never, ever), age at menarche (≤13, 14, 15, ≥16 years, or missing), age at first birth (nulliparous, <26 years, ≥26 years, or missing), parity (nulliparous, 1–2 times, 3 times, and ≥4 times, or missing), age at menopause (pre, ≤44, 45–54, ≥55 years), use of exogenous female hormones (ever, never), alcohol intake (non-/past-/occasional drinkers, regular drinkers ≤150 or >150 ethanol g/week), and energy-adjusted intake of isoflavones (continuous) and daily total physical activity (tertile of METs or missing).
[e] Multivariable Cox proportional hazards models were adjusted for age (time-scales), area (10), height (continuous), recent BMI (continuous), BMI at age 20 years (continuous), smoking status (never, ever), age at menarche (≤13, 14, 15, ≥16 years, or missing), age at menopause (pre, ≤44, 45–54, ≥55 years), use of exogenous female hormones (ever, never), alcohol intake (non-/past-/occasional drinkers, regular drinkers), and energy-adjusted intake of isoflavones (continuous) and daily total physical activity (tertile of MET or missing).
[f] Participation frequency in leisure-time physical activity was categorized (≤ 3 days/month vs. ≥1 day/week).

Table 3
Relative risks (RRs) and 95% confidence intervals (CIs) for the association between daily total physical activity (DTPA) level and breast cancer risk among Japanese women in the Japan Public Health Center-based Prospective Study (Cohort II), 1990–2007.

	All					Premenopausal women[b]					Postmenopausal women[c]				
	DTPA (METs/day score)					DTPA (METs/day score)					DTPA (METs/day score)				
	Cases/*n*	Tertile 1 Ref.	Tertile 2 RR (95% CI)	Tertile 3 RR (95% CI)	p_{trend}	Cases/*n*	Tertile 1 Ref.	Tertile 2 RR (95% CI)	Tertile 3 RR (95% CI)	p_{trend}	Cases/*n*	Tertile 1 Ref.	Tertile 2 RR (95% CI)	Tertile 3 RR (95% CI)	p_{trend}
Total person-years		128960	143178	152199			46084	57485	53928			82875	85694	98270	
All		106	92	96			41	44	43			65	48	53	
Model[a]	294/31917	1.00 (ref.)	1.08 (0.82–1.43)	0.90 (0.68–1.19)	0.48	128/11953	1.00 (ref.)	1.07 (0.70–1.65)	0.86 (0.56–1.32)	0.48	166/19964	1.00 (ref.)	1.07 (0.73–1.55)	0.93 (0.65–1.34)	0.72
		82	70	76			35	40	35			47	30	41	
Model[d]	228/23977	1.00 (ref.)	1.13 (0.82–1.56)	1.03 (0.75–1.41)	0.86	110/9979	1.00 (ref.)	1.24 (0.78–1.97)	0.89 (0.55–1.43)	0.61	118/13998	1.00 (ref.)	1.02 (0.64–1.63)	1.11 (0.72–1.70)	0.65
ER+PR+		22	32	43			4	5	5			18	5	6	
Model[a]	43/31917	1.00 (ref.)	0.61 (0.29–1.30)	0.57 (0.27–1.17)	0.11	14/11953	1.00 (ref.)	1.35 (0.36–5.04)	1.19 (0.31–4.56)	0.81	29/19964	1.00 (ref.)	0.42 (0.16–1.13)	0.43 (0.17–1.08)	0.046
ER+PR−		7	10	5			4	4	3			3	6	2	
Model[a]	22/31917	1.00 (ref.)	1.94 (0.73–5.18)	0.79 (0.25–2.50)	0.74	11/11953	1.00 (ref.)	1.03 (0.26–4.12)	0.59 (0.13–2.64)	0.49	11/19964	1.00 (ref.)	3.87 (0.89–16.91)	0.98 (0.16–5.91)	0.88
ER−PR−		4	8	9			2	3	2			2	5	7	
Model[a]	21/31917	1.00 (ref.)	2.38 (0.71–7.93)	2.36 (0.72–7.70)	0.17	7/11953	1.00 (ref.)	1.58 (0.26–9.46)	0.90 (0.13–6.37)	0.90	14/19964	1.00 (ref.)	3.20 (0.62–16.55)	4.17 (0.86–20.14)	0.07
Unknown		71	64	70			31	32	32			40	32	38	
Model[a]	205/31917	1.00 (ref.)	1.10 (0.79–1.55)	0.95 (0.68–1.32)	0.73	95/11953	1.00 (ref.)	1.01 (0.62–1.66)	0.83 (0.50–1.36)	0.44	110/19964	1.00 (ref.)	1.14 (0.72–1.82)	1.03 (0.66–1.61)	0.90

[a] Cox proportional hazards models was adjusted for age (time-scales) and area (10).
[b] For premenopausal women, multivariable Cox proportional hazards models were adjusted for all following covariates (d or e) except age at menopause.
[c] For postmenopausal women, multivariable Cox proportional hazards models were adjusted for all following covariates (d or e) and age at menopause (≤44, 45–54, ≥55 years).
[d] Multivariable Cox proportional hazards models were adjusted for age (time-scales), area (10), height (continuous), recent BMI (continuous), BMI at age 20 years (continuous), smoking status (never, ever), age at menarche (≤13, 14, 15, ≥16 years, or missing), age at first birth (nulliparous, <26 years, ≥26 years, or missing), parity (nulliparous, 1–2 times, 3 times, and ≥4 times, or missing), age at menopause (pre, ≤44, 45–54, ≥55 years), use of exogenous female hormones (ever, never), alcohol intake (non-/past-/occasional drinkers, regular drinkers ≤150 or >150 ethanol g/week), and energy-adjusted intake of isoflavones (continuous) and participation frequency in leisure-time physical activity (≤3 days/month, 1–2 days/week, ≥3 days/week).

Table 4
Relative risks (RRs) and 95% confidence intervals (CIs) for the association between leisure-time physical activity and hormone receptor status-defined breast cancer risk stratified by BMI in the Japan Public Health Center-based Prospective Study 1990–2007.

Type of tumor	BMI <25 (n=38,959)				BMI ≥25 (n=14,619)			
	Cases	Leisure-time physical activity			Cases	Leisure-time physical activity		
		≤3 days/month	≥1 day/week			≤3 days/month	≥1 day/week	
		Ref.	RR (95% CI)	p_{trend}		Ref.	RR (95% CI)	p_{trend}
Person-years		454047	110033			173623	42391	
		359	94			170	29	
All[a]	453/38959	1.00 (ref.)	1.02 (0.81–1.28)	0.90	199/14619	1.00 (ref.)	0.65 (0.43–0.97)	0.033
		75	15			40	5	
ER+PR+[a]	90/38959	1.00 (ref.)	0.84 (0.48–1.48)	0.55	45/14619	1.00 (ref.)	0.50 (0.20–1.27)	0.14
		32	12			18	2	
ER+PR−[a]	44/38959	1.00 (ref.)	1.61 (0.82–3.16)	0.17	20/14619	1.00 (ref.)	0.51 (0.12–2.23)	0.37
		51	14			15	3	
ER−PR−[a]	65/38959	1.00 (ref.)	1.11 (0.61–2.01)	0.74	18/14619	1.00 (ref.)	0.93 (0.27–3.27)	0.91
		192	49			93	19	
Unknown[a]	241/38959	1.00 (ref.)	0.92 (0.67–1.26)	0.6	112/14619	1.00 (ref.)	0.72 (0.43–1.18)	0.19

[a] Cox proportional hazards models were adjusted for age (time-scales), area (10).

considered. Nevertheless, RR for unknown tumors was similar to that for overall tumors, suggesting that there was little bias in our results. Further, our information on LPA included frequency only and not intensity or duration. Finally, we are unable to rule out the possibility of a chance finding, measurement error in exposure information due to self-reporting, and residual confounding due to unmeasured/unknown information.

Conclusion

LPA was associated with a decreased risk of breast cancer in overall and postmenopausal ER+PR+ tumors. Among overweight women, a substantially decreased risk with LPA was observed. We also observed a substantial inverse trend between DTPA and postmenopausal ER+PR+ tumors, although DTPA was not associated with overall breast cancer risk. Active participation in LPA might represent a useful public health message against breast cancer, particularly among elderly women, given that the majority of breast tumors occurring after menopause are ER+PR+ tumors.

Funding

This work was supported by the Ministry of Health, Labour and Welfare of Japan [grants-in-aid for Cancer Research (No. 19 shi-2)], [grants-in-aid for the 3rd term Comprehensive 10-Year Strategy for Cancer Control (H21-Sanjigan-Ippan-003)], by the Ministry of Education, Culture, Sports, Science, and Technology of Japan [grants-in-aid for Scientific Research on Priority Area (17015049)], and by Management Expenses Grants from the Government to the National Cancer Center. RS is an awardee of a Research Resident Fellowship from the Foundation for Promotion of Cancer Research (Japan) for the 3rd term Comprehensive 10-Year Strategy for Cancer Control.

Conflict of interest statement
The authors declare that there are no conflicts of interest.

Acknowledgments

We thank all staff members in each study area and in the central offices for their cooperation and technical assistance. We also wish to thank the Iwate, Aomori, Ibaraki, Niigata, Osaka, Kochi, Nagasaki and Okinawa Cancer Registries for their provision of incidence data.

Appendix

Members of the Japan Public Health Center-based Prospective Study Group (principal investigator: S. Tsugane): S. Tsugane, M. Inoue, T. Sobue, and T. Hanaoka, National Cancer Center, Tokyo; J. Ogata, S. Baba, T. Mannami, A. Okayama, and Y. Kokubo, National Cardiovascular Center, Osaka; K. Miyakawa, F. Saito, A. Koizumi, Y. Sano, I. Hashimoto, and T. Ikuta, Iwate Prefectural Ninohe Public Health Center, Iwate; Y. Miyajima, N. Suzuki, S. Nagasawa, Y. Furusugi, and N. Nagai, Akita Prefectural Yokote Public Health Center, Akita; H. Sanada, Y. Hatayama, F. Kobayashi, H. Uchino, Y. Shirai, T. Kondo, R. Sasaki, Y. Watanabe, Y. Miyagawa, and Y. Kobayashi, Nagano Prefectural Saku Public Health Center, Nagano; Y. Kishimoto, E. Takara, T. Fukuyama, M. Kinjo, M. Irei, and H. Sakiyama, Okinawa Prefectural Chubu Public Health Center, Okinawa; K. Imoto, H. Yazawa, T. Seo, A. Seiko, F. Ito, and F. Shoji, Katsushika Public Health Center, Tokyo; A. Murata, K. Minato, K. Motegi, and T. Fujieda, Ibaraki Prefectural Mito Public Health Center, Ibaraki; K. Matsui, T. Abe, M. Katagiri, and M. Suzuki, Niigata Prefectural Kashiwazaki and Nagaoka Public Health Center, Niigata; M. Doi, A. Terao, Y. Ishikawa, and T. Tagami, Kochi Prefectural Chuo-higashi Public Health Center, Kochi; H. Sueta, H. Doi, M. Urata, N. Okamoto, and F. Ide, Nagasaki Prefectural Kamigoto Public Health Center, Nagasaki; H. Sakiyama, N. Onga, H. Takaesu, and M. Uehara, Okinawa Prefectural Miyako Public Health Center, Okinawa; F. Horii, I. Asano, H. Yamaguchi, K. Aoki, S. Maruyama, M. Ichii, and M. Takano, Osaka Prefectural Suita Public Health Center, Osaka; S. Matsushima and S. Natsukawa, Saku General Hospital, Nagano; K. Suzuki, Research Institute for Brain and Blood Vessels Akita, Akita; M. Kabuto, National Institute for Environmental Studies, Ibaraki; M. Yamaguchi, Y. Matsumura, S. Sasaki, and S. Watanabe, National Institute of Health and Nutrition, Tokyo; M. Noda, International Medical Center of Japan, Tokyo; S. Tominaga, Aichi Cancer Center Research Institute, Aichi; H. Shimizu, Sakihae Institute, Gifu; M. Iida, W. Ajiki, and A. Ioka, Osaka Medical Center for Cancer and Cardiovascular Disease, Osaka; S. Sato, Osaka Medical Center for Health Science and Promotion, Osaka; Y. Tsubono, Tohoku University, Miyagi; K. Nakamura, Niigata University, Niigata; Y. Honda, K. Yamagishi, and S. Sakurai, Tsukuba University, Ibaraki; M. Akabane, Tokyo University of Agriculture, Tokyo; T. Kadowaki, Tokyo University, Tokyo; Y. Kawaguchi, Tokyo Medical and Dental University, Tokyo; Y. Takashima, Kyorin University, Tokyo; H. Sugimura, Hamamatsu University, Shizuoka; H. Iso, Osaka University, Osaka; E. Maruyama, Kobe University, Hyogo; M. Konishi, K. Okada, and I. Saito, Ehime University, Ehime; N. Yasuda, Kochi University, Kochi; and S. Kono, Kyushu University, Fukuoka.